Biophysical studies of the *Burkholderia* minor translocon protein BipC by NMR and CD spectroscopy

By

Sanjay K. Yadava

Submitted to the Graduate Degree Program in the

Department of Molecular Biosciences and the Graduate Faculty

of the University of Kansas in partial fulfillment of the requirements for the degree

of Master of Arts

Chairperson: Roberto N. De Guzman, Ph.D.

Committee Members: Mark Richter, Ph.D.

Susan Egan, Ph.D.

Date Defended: 05/12/2017

The Thesis Committee for Sanjay K. Yadava certifies that this is the approved version of the following Thesis:

Biophysical studies of the *Burkholderia* minor translocon protein BipC by NMR and CD spectroscopy

Chairperson: Roberto N. De Guzman, Ph.D.

Date Approved: 05/24/2017

Abstract

The type III secretion system (T3SS) provides many Gram-negative pathogens a tool to initiate, maintain and proliferate infection in the host. The T3SS is a syringe-like apparatus composed of a base that transverses the bacterial membranes, an extracellular needle, a tip complex, and a translocon. The T3SS consists of over 20 different protein components that assemble to form a pore into the host membrane. The T3SS creates a pathway for the transport of bacterial effector molecules into the host cytoplasm. The effector molecules hijack and manipulate the host cytoskeleton and cell signaling pathways to promote invasion by the bacteria, circumvention of the host immune system, and maintenance of infection.

Several Gram-negative pathogens utilize the T3SS for infection including *Burkholderia pseudomallei* (melioidosis), *Salmonella typhimurium* (infectious diarrhea/typhoid), *Shigella flexneri* (shigellosis), *Pseudomonas aeruginosa* (nosocomial infection), *Yersinia pestis* (bubonic plague), *Chlamydia trachomatis* (sexually transmitted disease), and enterohemorrahagic *Escherichia coli* (bloody diarrhea/urinary tract infection). These pathogens pose a serious threat to public health, when combined they cause millions of cases of illness and deaths and constitute a huge economical burden to the US and the rest of the world.

Since its discovery and visualization about two decades ago, the bacterial T3SS has enticed intense scientific research focused on deciphering the assembly of the injectisome, its virulence mechanism and discovery or design of novel vaccines and anti-infectives. The needle-tip-translocon proteins of the T3SS are potential therapeutic

targets because of their hydrophilicity and exposure to the extracellular space. The needle and the tip proteins in *Salmonella* and *Shigella* have been characterized but the assembly of the translocon proteins and tip-translocon interaction has not been extensively studied. This thesis explores the *Burkholderia* tip-translocon protein-protein interaction and the interaction of the translocon with a membrane. I utilized biophysical techniques namely solution nuclear magnetic resonance (NMR) and circular dichroism (CD) spectroscopy to investigate the protein binding surfaces involved in tip-translocon interaction as well as the structural transition of the translocon protein on exposure to membrane mimic detergent micelles. I have herein shown that the *Burkholderia* minor translocon protein BipC might be binding at the mixed α-β region of the tip protein BipD extrapolated from the interaction study between BipC and BipD as well as its homologs *Salmonella* SipD and *Shigella* IpaD. The results help understand the interaction of the *Burkholderia* minor translocon protein with the tip protein and detergent micelles and thus add to the knowledge of T3SS assembly.

Acknowledgements

I would foremost like to thank my family for their support and encouragement throughout the years. This would not be possible without the unwavering motivation and confidence shown in me by my family. They have been the cornerstone and the only constant during all the struggles in my life.

I am especially thankful to my mentor Dr. Roberto N. De Guzman for providing me with guidance and support during the pursuit of my Master's degree. He would always offer constructive criticism that has shaped my graduate career as well as my overall personality development.

I thank my committee members Dr. Mark Richter, Dr. Susan Egan, Dr. David Davido, Dr. Krzysztof Kuczera, and Dr. Chris Fischer for their feedback and input that proved invaluable in the completion of this thesis and my graduate education.

I would also like to thank the former members of the lab Dr. Andrew McShan and Dr. Kawaljit Kaur, as well as the current members of the lab Dr. Supratim Dey, Amritangshu Chakravarty, Pallavi Guha Biswas, and Mason Wilkinson.

I would like to acknowledge Dr. Justin T. Douglas and Dr. Minli Xing from the KU NMR core facility for their help with the NMR instruments and acquisition of data. I would also like to acknowledge Dr. Philip Gao from the KU Protein Production Group for valuable suggestion in analyzing some of the NMR data.

Lastly, I thank everyone who might have influenced me in one way or the other during my time at the University of Kansas. I look forward to utilizing the skills and lessons learned during my graduate study in the future endeavors.

Table of Contents

List of Figures

Figure..... Page

List of tables

List of Abbreviations

T3SS	Type III Secretion System
EPEC	Enteropathogenic *Escherichia coli*
GB1	*Streptococcus* protein G B1 domain
TEV	Tobacco Etch Virus
IPTG	Isopropyl-β-D-thiogalactopyrandoside
LB	Lysogeny Broth
TB	Terrific Broth
NMR	Nuclear Magnetic Resonance
TROSY	Transverse Optimized Relaxation Spectroscopy
HSQC	Heteronuclear Single Quantum Coherence
CD	Circular Dichroism
CMC	Critical Micelle Concentration
DPC	Dodecylphosphocholine
LMPG	Lyso-myristoylphosphatidylglycerol
T3SA	Type III Secretion Apparatus
MCS	Multiple cloning site
Ni-NTA	Nickel-nitrilotriacetic acid
TM	Transmembrane

Chapter 1: Introduction

1.1. Introduction to the type III secretion system

Bacterial pathogens interact with host to cause disease and in the process have evolved different strategies to overcome host defense systems [1]. These pathogens utilize various virulence factors to undermine the host cell response in order to establish infection [2]. The interaction between bacterial pathogens and their hosts is a tug of war in which both try to outsmart each other and in the process evolve new infection and defense mechanisms [3, 4]. Bacterial pathogens have evolved protein secretion apparati that deliver virulence effector molecules into the host cell sabotaging host cellular processes such as cytoskeleton rearrangement and cell signaling pathways [3, 4].

The secretion of proteins in Gram-positive bacteria is carried out through the general secretory pathway in a sec-dependent manner [1, 5]. Many Gram-negative bacteria have evolved specialized secretion systems to overcome the hurdle posed by the presence of an outer membrane [1, 5]. One such system is the type III secretion system (T3SS) that shares similarity with the flagellar assembly apparatus [6, 7]. This secretion apparatus is harbored by animal pathogens including the causative agents of melioidosis (*Burkholderia pseudomallei*), infectious diarrhea/enteric fever (*Salmonella typhimurium),* shigellosis (*Shigella flexneri)*, nosocomial infections (*Pseudomonas aeruginosa*), plague (*Yersinia pestis*), and bloody diarrhea/urinary tract infection (enterohemorrahagic *Escherichia coli*) as well as plant pathogens such as *Erwinia* spp, and *Xanthomonas* spp [4, 8, 9]. Additionally, the evolution of antibacterial resistance in these pathogens presents a global threat to human health [10, 11, 12]. Pathogens like

Yersinia and *Burkholderia* are listed as Category A and Category B potential bio-threat agents, respectively, by the Centers for Disease Control and Prevention as well as the National Institute of Allergy and Infectious Diseases[13, 14, 15]. As such, the understanding of the structural and functional aspects of T3SS in pathogenesis is vital to the development of novel vaccines, anti-infectives and alternative therapeutics.

Burkholderia pseudomallei is a Gram-negative pathogen and the causative agent of melioidosis. It has been identified to harbor three T3SS encoding genetic loci in distinct pathogenicity islands [16, 17, 18, 19]. Of these, the T3SS1 and T3SS2 share homology to the plant pathogens *Ralstonia solanacearum* and *Xanthomonas* spp while T3SS3 is homologous to the Inv/Mxi-Spa systems of *Salmonella* and *Shigella* involved in infection in animals [16, 17].

The T3SS broadly consists of a base traversing the bacterial inner and outer membranes, a needle extending into the extracellular space, a tip protein, and a translocon pore into the host membrane formed by two translocator proteins (Fig. 1-1). The T3SSs in *Burkholderia* and other bacterial species are structurally and functionally conserved systems made up of more than 20 different proteins [20, 21, 22] (Table 1-1 and Figure 1-2). The two translocon proteins are essential for the formation of an opening into the host cell establishing a conduit enabling the export of virulence effector molecules into the host cytoplasm. The structures of the N-terminal domains of the major translocon proteins SipB from *Salmonella* and IpaB from *Shigella* are known [23]. Others have shown the interaction between the major translocon proteins from *Salmonella* and *Shigella* and their respective tip proteins [24, 25].

The minor translocon protein is important in puncturing a pore into the host membrane and is indispensable for bacterial capacity to cause infection [26, 27]. The interaction of the minor translocon proteins with the tip proteins and the host membrane is not known. This thesis investigates the tip-translocon protein-protein interaction and the translocon-membrane interaction by nuclear magnetic resonance (NMR) and circular dichroism (CD) spectroscopy. Chapter 2 of this thesis describes the interaction of the *Burkholderia* minor translocon protein BipC with the *Burkholderia* tip protein BipD and its homologs *Salmonella* SipD and *Shigella* IpaD while Chapter 3 is dedicated to the characterization of BipC interaction with membrane mimetic detergents.

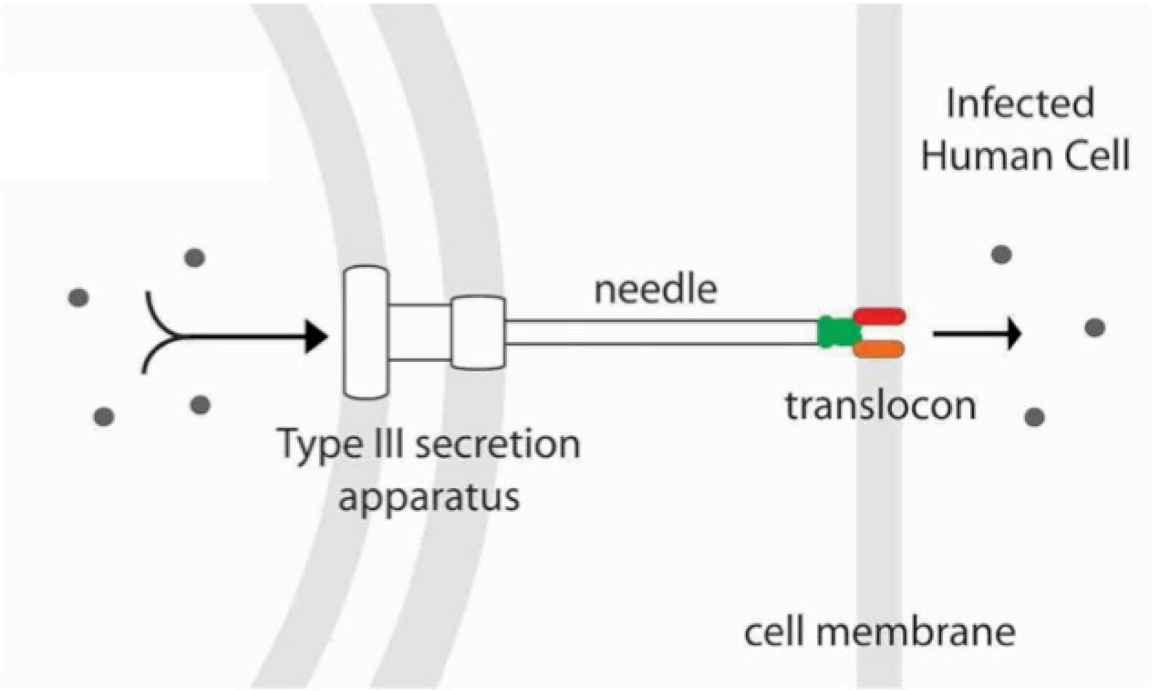

Alejandro Heuk Laboratory, University of Massachusetts, Amherst

Figure 1-1. A cartoon representation of T3SS in Gram-negative pathogens including *Burkholderia.* The syringe-like apparatus consists of a base embedded in the inner and outer bacterial membranes, an extracellular needle, a tip complex, and a translocon.

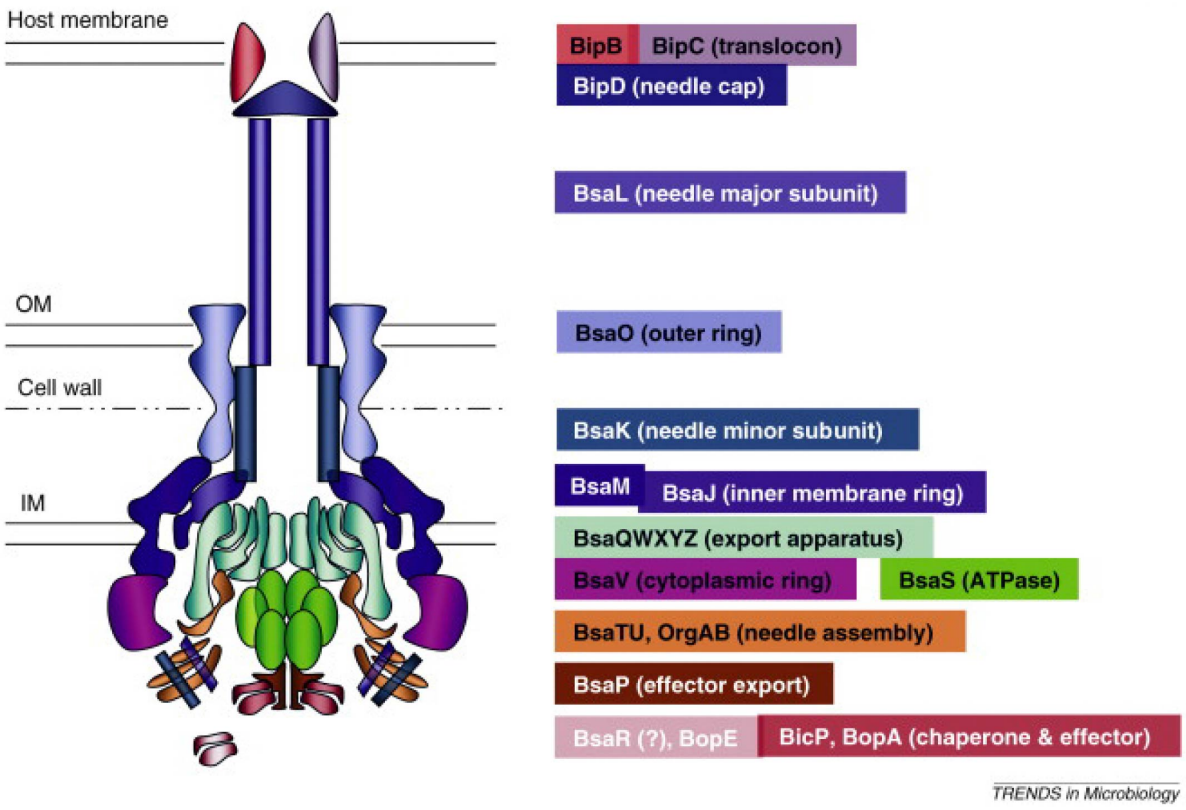

Figure. 1-2. A proposed model of T3SS in *Burkholderia.* The different components of T3SS are color-coded and are not drawn to scale. This figure is taken from *Sun et al* [1].

Table 1-1. List of homologous proteins of T3SS of various Gram-negative pathogens. Compiled and adapted from *Sun et al, Trends Microbiol, 2010* and *Chatterjee et al*, *Biochemistry, 2010.*

Role	*Burkholderia*	*Salmonella*	*Shigella*	*Yersinia*	*EPEC*	*Pseudomonas*
translocon	BipB	SipB	IpaB	YopB	EspB	PopB
translocon	BipC	SipC	IpaC	YopD	EspD	PopD
needle tip	BipD	SipD	IpaD	LcrV	EspA	PcrV
needle	BsaL	PrgI	MxiH	YscF	EscF	PscF
OM ring	BsaO	InvG	MxiD	YscC	EscC	PscC
inner rod	BsaK	PrgJ	MxiI	YscI	EscI	PscI
IM ring	BsaJ/BsaM	PrgK/PrgH	MxiJ/MxiG	YscJ/YscD	EscJ/EscD	PscJ/PscD
export apparatus	BsaW	SpaP	Spa24	YscR	EscR	PscR
	BsaX	SpaQ	Spa9	YscS	EscS	PscS
	BsaY	SpaR	Spa29	YscT	EscT	PscT
	BsaZ	SpaS	Spa40	YscU	EscU	PscU
	BsaQ	InvA	MxiA	YscV	EscV	PcrD
ATPase	BsaS	InvC	Spa47	YscN	EscN	PscN

1.2. References

[1] Galan, J. E., and Bliska, J. B. (1996) Cross-talk between bacterial pathogens and their host cells, *Annu Rev Cell Dev Biol 12*, 221-255.

[2] Bliska, J. B., Galan, J. E., and Falkow, S. (1993) Signal transduction in the mammalian cell during bacterial attachment and entry, *Cell 73*, 903-920.

[3] Salmond, G. P., and Reeves, P. J. (1993) Membrane traffic wardens and protein secretion in gram-negative bacteria, *Trends Biochem Sci 18*, 7-12.

[4] Van Gijsegem, F., Genin, S., and Boucher, C. (1993) Conservation of secretion pathways for pathogenicity determinants of plant and animal bacteria, *Trends Microbiol 1*, 175-180.

[5] Gerlach, R. G., and Hensel, M. (2007) Protein secretion systems and adhesins: the molecular armory of Gram-negative pathogens, *Int J Med Microbiol 297*, 401-415.

[6] Pallen, M. J., Beatson, S. A., and Bailey, C. M. (2005) Bioinformatics, genomics and evolution of non-flagellar type-III secretion systems: a Darwinian perspective, *FEMS Microbiol Rev 29*, 201-229.

[7] Abby, S. S., and Rocha, E. P. (2012) The non-flagellar type III secretion system evolved from the bacterial flagellum and diversified into host-cell adapted systems, *PLoS Genet 8*, e1002983.

[8] Coburn, B., Sekirov, I., and Finlay, B. B. (2007) Type III secretion systems and disease, *Clin Microbiol Rev 20*, 535-549.

[9] Notti, R. Q., and Stebbins, C. E. (2016) The Structure and Function of Type III Secretion Systems, *Microbiol Spectr 4*.

[10] Wellington, E. M., Boxall, A. B., Cross, P., Feil, E. J., Gaze, W. H., Hawkey, P. M., Johnson-Rollings, A. S., Jones, D. L., Lee, N. M., Otten, W., Thomas, C. M., and Williams, A. P. (2013) The role of the natural environment in the emergence of antibiotic resistance in gram-negative bacteria, *Lancet Infect Dis 13*, 155-165.

[11] Allen, H. K., Donato, J., Wang, H. H., Cloud-Hansen, K. A., Davies, J., and Handelsman, J. (2010) Call of the wild: antibiotic resistance genes in natural environments, *Nat Rev Microbiol 8*, 251-259.

[12] Davies, J., and Davies, D. (2010) Origins and evolution of antibiotic resistance, *Microbiol Mol Biol Rev 74*, 417-433.

[13] Ruppitsch, W., Stoger, A., Indra, A., Grif, K., Schabereiter-Gurtner, C., Hirschl, A., and Allerberger, F. (2007) Suitability of partial 16S ribosomal RNA gene sequence analysis for the identification of dangerous bacterial pathogens, *J Appl Microbiol 102*, 852-859.

[14] Cheng, A. C., and Currie, B. J. (2005) Melioidosis: epidemiology, pathophysiology, and management, *Clin Microbiol Rev 18*, 383-416.

[15] Tian, D., and Zheng, T. (2014) Comparison and analysis of biological agent category lists based on biosafety and biodefense, *PLoS One 9*, e101163.

[16] Sun, G. W., and Gan, Y.-H. (2010) Unraveling type III secretion systems in the highly versatile Burkholderia pseudomallei, *Trends in Microbiology 18*, 561-568.

[17] Zhang, L., Wang, Y., Picking, W. L., Picking, W. D., and De Guzman, R. N. (2006) Solution structure of monomeric BsaL, the type III secretion needle protein of Burkholderia pseudomallei, *J Mol Biol 359*, 322-330.

[18] Stevens, M. P., Wood, M. W., Taylor, L. A., Monaghan, P., Hawes, P., Jones, P. W., Wallis, T. S., and Galyov, E. E. (2002) An Inv/Mxi-Spa-like type III protein secretion system in Burkholderia pseudomallei modulates intracellular behaviour of the pathogen, *Mol Microbiol 46*, 649-659.

[19] Winstanley, C., Hales, B. A., and Hart, C. A. (1999) Evidence for the presence in Burkholderia pseudomallei of a type III secretion system-associated gene cluster, *J Med Microbiol 48*, 649-656.

[20] Moraes, T. F., Spreter, T., and Strynadka, N. C. (2008) Piecing together the type III injectisome of bacterial pathogens, *Curr Opin Struct Biol 18*, 258-266.

[21] Galan, J. E., and Wolf-Watz, H. (2006) Protein delivery into eukaryotic cells by type III secretion machines, *Nature 444*, 567-573.

[22] Chatterjee, S., Chaudhury, S., McShan, A. C., Kaur, K., and De Guzman, R. N. (2013) Structure and biophysics of type III secretion in bacteria, *Biochemistry 52*, 2508-2517.

[23] Barta, M. L., Dickenson, N. E., Patil, M., Keightley, A., Wyckoff, G. J., Picking, W. D., Picking, W. L., and Geisbrecht, B. V. (2012) The structures of coiled-coil

domains from type III secretion system translocators reveal homology to pore-forming toxins, *J Mol Biol 417*, 395-405.

[24] McShan, A. C., Kaur, K., Chatterjee, S., Knight, K. M., and De Guzman, R. N. (2016) NMR identification of the binding surfaces involved in the Salmonella and Shigella Type III secretion tip-translocon protein-protein interactions, *Proteins 84*, 1097-1107.

[25] Kaur, K., Chatterjee, S., and De Guzman, R. N. (2016) Characterization of the Shigella and Salmonella Type III Secretion System Tip-Translocon Protein-Protein Interaction by Paramagnetic Relaxation Enhancement, *Chembiochem 17*, 745-752.

[26] Picking, W. L., Coye, L., Osiecki, J. C., Barnoski Serfis, A., Schaper, E., and Picking, W. D. (2001) Identification of functional regions within invasion plasmid antigen C (IpaC) of Shigella flexneri, *Mol Microbiol 39*, 100-111.

[27] Job, V., Mattei, P. J., Lemaire, D., Attree, I., and Dessen, A. (2010) Structural basis of chaperone recognition of type III secretion system minor translocator proteins, *J Biol Chem 285*, 23224-23232.

Chapter 2: Mapping of the binding surface of the minor translocon protein BipC on the tip protein BipD from the *Burkholderia* type III secretion system

2.1. Introduction

Burkholderia pseudomallei is a Gram-negative pathogen that infects a wide range of hosts from plants to animals, including humans [1, 2]. It is the causative agent of melioidosis that is prevalent and endemic in South-east Asia and north Australia [1, 2]. The clinical manifestation of melioidosis includes joint pain, acute or chronic pneumonia, septic shock, and organ abscess [1, 3]. The primary mode of infection is through direct contact with contaminated soil and water but one can also get the infection by inhaling contaminated dust and water droplets. Thus, it has been listed as a potential category B bioterrorism agent by the US Centers for Disease Control and Prevention [1, 4]. Lack of vaccines and the emergence of antibacterial resistant strains pose a major risk to public health particularly in areas hyperendemic for melioidosis-related septicemia [5]. *Burkholderia pseudomallei* like many other Gram-negative pathogens uses a common mechanism of infection, the type III secretion system (T3SS) [6]. The T3SS is a syringe like nano-injector that consists of a base spanning the bacterial inner and outer membranes, an extracellular needle protruding out of the cell, a tip protein, and a translocon that assembles a pore into the host membrane and thus forms a conduit for the passage of bacterial virulence effectors from within the bacteria directly into the host cell [7]. Three T3SSs have been identified in *Burkholderia pseudomallei* [8, 9, 10]. T3SS1 and T3SS2 are homologous to the plant pathogens *Ralstonia solanacearum* and

Xanthomonas spp while T3SS3 is homologous to the Inv/Mxi-Spa systems of *Salmonella* and *Shigella* and is required for infection in animals [8, 9, 10].

The T3SS has gained the attention of scientific research since its discovery about two decades ago [11]. The understanding of the T3SS is important to decode the structure-function relationship, mechanism of infection, and discovery of small molecule inhibitors that will specifically target protein-protein interactions required for the assembly of this nano-injector. The external hydrophilic part of the T3SS in particular offers a potential target for the discovery of small molecule inhibitors [12]. The structures of the needle and the tip proteins are known in well-studied systems such as *Salmonella*, *Shigella,* and *Burkholderia* [13]. The homologous tip proteins from *Salmonella* (SipD), *Shigella* (IpaD), and *Burkholderia* (BipD) contain an N-terminal α-helical hairpin, a central-coiled-coil domain, and a distal region of mixed α-helices and β-strands (Figure 2-1) [13]. The *Burkholderia* BipD shares ~26% identity and ~39% similarity to *Salmonela* SipD while ~26% identity and ~37% similarity to *Shigella* IpaD [14, 15, 16] (Figure 2-2). However, the structures of the translocons and the interaction between the tip and the translocons, particularly the minor translocon is not known. My work involves elucidating the tip-translocon interaction, and in this study I have provided evidence that the minor translocon BipC from *Burkholderia* may be binding at the mixed α-β domain of the tip protein, BipD from *Burkholderia* and its homologs *Salmonella* SipD and *Shigella* IpaD.

2.2. Experimental Section

2.2.1. Expression and purification of ^{15}N-and ILV-labeled and unlabeled BipC, SipD, and IpaD

Full length BipC was cloned and amplified from *Burkholderia pseudomallei* strain K96243 and subsequently sub-cloned into pET-22b using the NdeI and BamHI cloning sites (Dr. Supratim Dey). The tip proteins SipD$^{39\text{-}343}$ and IpaD$^{38\text{-}332}$ from *Salmonella typhimurium* strain SL1344 and *Shigella flexneri* respectively were previously subconed into a modiefied pET-21a expression vector [13, 17]. All the protein constructs contain an N-terminal 6X-His tag, GB1 (B1 domain of the immunoglobulin binding protein G) solubility tag, and a TEV (Tobacco etch virus) protease cleavage site [18]. The BipC construct was transformed into *E. coli* BL21-CodonPlus (DE3)-RIPL strain (Agilent technologies). SipD$^{39\text{-}343}$ and IpaD$^{38\text{-}332}$ were transformed into *E. coli* BL21 (DE3)-DNAY cells. Uniformly ^{15}N-labeled BipC, SipD$^{39\text{-}343}$ and IpaD$^{38\text{-}332}$ were expressed in 1 liter of 1X Minimal media at 37 °C using the antibiotics, 100 ug/mL carbenicllin and 25 ug/mL chloramphenicol supplemented with 1 g/L $^{15}NH_4Cl$ as the sole source of nitrogen [19] until an OD_{600} ~ 0.8 after which the culture was induced with 1 mM IPTG (isopropyl –D-1-thiogalactopyranoside) and grown overnight at 15 °C. For ILV-labeling the cell cultures were supplemented with ~0.5 mg of alpha-ketobutyric acid (labels the single terminal methyl ^{13}Cδ of isoleucine) and ~100 mg of alpha-ketoisovaleric acid (labels the terminal methyl ^{13}Cδ of leucine and ^{13}CϒC of valine) at on OD_{600} ~0.4. Unlabeled BipC, SipD$^{39\text{-}343}$ and IpaD$^{38\text{-}332}$ were expressed in 1 liter of lysogeny broth (LB) or terrific broth (TB) media [19] at 37 °C using the antibiotics, 100 ug/mL carbenicllin and 25 ug/mL

chloramphenicol until an OD_{600} ~ 0.8 after which the cultures were induced with 1 mM IPTG. The next day, cells were harvested by centrifugation at ~3300 rcf for ~10 mins, re-suspended in binding buffer containing 5 mM imidazole, 20 mM Tris-HCl, 500 mM NaCl, pH 8.0, and 0.2 mM phenylmethanesulfonyl fluoride and lysed by sonication.

The sonicated cell cultures were centrifuged at ~20000 rcf for ~ 10 mins to remove any non-lysed cell debris from the cell lysate, mixed with ~ 0.1 mM polyethylenimine (PEI) solution to precipitate DNA matter and centrifuged again at ~20000 rcf for ~ 10 min to separate the soluble protein fractions from the DNA precipitate. The soluble fractions were then loaded on to a nickel affinity column packed with nickel-nitrilotriacetic acid (Ni-NTA) resin, washed three times with a buffer containing 20 mM Tris-HCl, 500 mM NaCl, 10mM imidazole, pH 8.0 to rid the column of non-binding contaminating proteins followed by elution of the 6X-His-GB1-BipC with 20 mM Tris-HCl, 500 mM NaCl, 250 mM imidazole, pH 8.0 elution buffer. The elution fraction containing the fusion protein was treated with TEV protease [20, 21] overnight in 20 mM Tris-HCl (pH8.0), 0.5 mM EDTA, 1 mM DTT, and 20 mM NaCl.

The TEV cleaved protein fraction was loaded on to a nickel affinity column, and then washed twice with a buffer containing 20 mM Tris-HCl, 500 mM NaCl, 40 mM imidazole to elute the cleaved BipC followed by the elution of the 6X-His-GB1 tag with 20 mM Tris HCl, 500 mM NaCl, 250 mM imidazole, pH 8.0. The wash fraction containing the BipC protein was exchanged by dialysis into NMR buffer (20 mM phosphate, 100 mM NaCl, pH 6.8) twice and then concentrated using Millipore centrifugal filter units with a 3000 MW cut off limit. The concentration of BipC was

estimated by the Bradford assay. The identification of BipC was verified by SDS PAGE gel electrophoresis and mass spectrometry.

2.2.2. NMR experiments

^{15}N-BipC titration with unlabeled BipD, SipD and IpaD

All NMR spectra were acquired using a Bruker Advance 800 MHz spectrometer equipped with a cryogenic triple resonance probe. NMR data were processed using NMRPipe [22] and analyzed using NMRView [23]. The acquisition parameters were 40 scans with ^{15}N sweep width of 30 ppm centered at 118 ppm and ^{1}H sweep width of 18 ppm centered at 4.7 ppm, 2048 ^{1}H complex points, and 400 ^{15}N complex points. Protein samples at varying molar ratios were prepared in NMR buffer (20mM phosphate, pH 6.8, 100mM NaCl, 10% D_2O), 500uL samples were placed in shigemi tubes and two dimensional ^{1}H-^{15}N-TROSY [24] experiments were recorded at 20 °C.

ILV- labeled BipC titration with unlabeled SipD

ILV-labeled BipC was titrated with unlabeled SipD dissolved in NMR buffer (20mM phosphate, pH 6.8, 100mM NaCl, 10% D_2O) to acquire two-dimensional ^{1}H-^{13}C HSQC spectra at 20 °C. The acquisition parameters used to acquire the 2D HSQC data were 16 scans, 1024 ^{1}H complex points and 180 ^{13}C complex points with ^{1}H sweep width of 12 ppm centered at 4.7 ppm, and ^{13}C sweep width of 22 ppm centered at 15 ppm.

^{15}N and ILV-labeled SipD and IpaD titration with unlabeled BipC

Two dimensional ^{1}H-^{15}N-TROSY [24] experiments were recorded for 0.1mM ^{15}N and ILV-labeled SipD$^{39-343}$ in NMR buffer (20mM phosphate, pH 6.8, 100mM NaCl, 10% D_2O) titrated with increasing concentrations of unlabeled BipC at 30 °C. The previously assigned amide peak list of SipD [25] was used to map the binding surface on the available PDB crystal structure of SipD (PDB ID: 3NZZ). The perturbed peaks from the ILV-titration experiments were also mapped onto the structure of SipD using previously ILV-assigned peak list of SipD [26].

Similarly, 0.13mM ^{15}N-labeled IpaD$^{38-332}$ was titrated with increasing concentrations of unlabeled BipC and the perturbed residues mapped onto the crystal structure of IpaD (PDB ID: 2J0O) using the previously assigned peak list of IpaD [27].

2.3 Results

2.3.1. BipC overexpression and purification

Uniformly ^{15}N-labeled BipC was overexpressed as a recombinant protein fused with His_6-GB1-TEV at the N-terminus in minimal media supplemented with $^{15}NH_4Cl$. The BipC construct expression was checked and verified by running the samples on an SDS polyacrylamide (PAGE) gel followed by purification from the soluble fraction by nickel affinity chromatography. The SDS PAGE and comassie blue staining verified efficient TEV cleavage separating the His_6-GB1 tag from the purified BipC protein (Figure 2-3). The purified BipC protein was also verified by mass spectrometry analysis (Figure 2-4).

2.3.2. ^{15}N/ILV-labeled BipC interaction with the tip proteins shown by NMR

The titration experiments for ^{15}N-labeled *Burkholderia* minor translocon protein BipC titrated with increasing concentrations of the unlabeled tip protein BipD$^{35\text{-}301}$ showed peak perturbation in the fast exchange NMR timescale as changes in peak position were observed indicating weak interaction (Figure 2-5). Similarly, the titration of ^{15}N-labeled BipC with BipD homologs, *Salmonella* SipD and *Shigella* IpaD showed perturbation of the same peaks and some new peaks in the fast exchange NMR timescale, although the chemical shift perturbation was on a smaller scale for SipD$^{39\text{-}343}$ and IpaD$^{38\text{-}332}$ compared to BipD$^{35\text{-}301}$ (Figure 2-6 and Figure 2-7). The difference in the extent of chemical shift perturbation could be due to the fact that BipD is the natural binding partner of BipC whereas SipD and IpaD are homologs from different bacterial species with only ~27% sequence identity. Therefore BipC perhaps binds comparatively stronger to BipD than either SipD or IpaD. The ILV-labeled BipC did not yield a good NMR spectrum as the majority of the Isoleucine, Leucine, and Valine peaks were missing and the resolution was poor. The titration of ILV-labeled BipC with unlabeled-SipD did not improve the spectral quality. As a result, ILV-labeled BipC titrations with the tip proteins were not further investigated.

2.3.3. ^{15}N-labeled tip protein interaction with BipC shown by NMR

The ^{15}N-labeled *Salmonella* tip protein SipD$^{39\text{-}343}$ titrated with unlabeled *Burkholderia* minor translocon protein BipC showed peak perturbation in the intermediate exchange on NMR timescale, as there were clear indications of reduction in peak intensities (Figure 2-8). The reduced peak intensity in the intermediate

exchange results due to a peak broadening phenomenon on interaction with BipC. The broader peaks and thus reduced peak intensity is observed when the exchange rate is in the range of the chemical shift difference between the bound and unbound state of the protein. The extent of perturbation was analyzed by quantifying the peak intensity ratio of the highest molar ratio to the lowest molar ratio titration. The peaks that were most perturbed were then mapped onto the structure of SipD (Figure 2-10). Likewise, the ILV-labeled SipD$^{39-343}$ titration with unlabeled BipC generated peak perturbation in the intermediate exchange on NMR timescale (Figure 2-9). The perturbed peaks were analyzed, quantified, and subsequently mapped on to the structure of SipD (Figure 2-10). Most of the highly perturbed residues from the ^{15}N and the ILV titration experiments were located in the distal region of SipD in the mixed α-β region while a few peaks also mapped on the coiled-coil domain.

Similarly, ^{15}N-labeled *Shigella* tip protein IpaD$^{38-332}$ was also titrated with increasing concentrations of unlabeled BipC. The peak perturbation was observed in the intermediate exchange on NMR timescale and the resulting peak intensities were quantified and mapped onto the structure of IpaD (Figure 2-11 and Figure 2-12). As previously found with SipD, most of the perturbed residues mapped to the distal region of IpaD in the mixed α-β region but some residues were located in the coiled-coil domain.

2.4. Discussion

The ^{15}N-labeled *Burkholderia* minor translocon protein BipC was titrated with the homologous tip proteins BipD$^{35-301}$, SipD$^{39-343}$, and IpaD$^{38-332}$ from *Burkholderia*,

Salmonella and *Shigella* respectively, at varying concentrations. The results provide evidence that BipC perhaps binds to the three tip proteins using a common binding surface, as the same peaks on BipC were perturbed in the titration experiments with the three tip proteins. Furthermore, the peak perturbations were observed in the fast exchange on NMR timescale, which indicates weak interaction. The bottleneck in this study at this juncture was that those peaks from BipC could not be identified because the NMR peak assignment of BipC is lacking. The reverse titration of ^{15}N-labeled BipD with unlabeled BipC was not feasible because the NMR spectrum of BipD has not been assigned either.

The alternative strategy used to overcome this dilemma was to titrate ^{15}N and ILV-labeled tip proteins SipD$^{39\text{-}343}$ and IpaD$^{38\text{-}332}$ with unlabeled BipC. *Burkholderia* BipD is homologous to *Salmonella* SipD and *Shigella* IpaD. BipD shares ~26% identity and ~39% similarity to SipD while ~27% identity and ~ 37% similarity to IpaD[*14*, *15*, *16*] (Figure 2-2). The NMR assignments for SipD$^{39\text{-}343}$ and IpaD$^{38\text{-}332}$ are available [*25*, *26*, *27*]. The ^{15}N and ILV-labeled SipD$^{39\text{-}343}$ titration with unlabeled BipC yielded peak perturbations in the intermediate exchange NMR timescale indicating weak interaction. The peaks that showed the highest perturbation were quantified, analyzed and then mapped onto the structure of SipD$^{39\text{-}343}$. The most perturbed peaks mapped onto the distal region of SipD$^{39\text{-}}$343 in the mixed α-β region while a few peaks were also located in the coiled-coil domain.

Likewise, titration experiments with ^{15}N-labeled IpaD$^{38\text{-}332}$ and unlabeled BipC were also performed. As seen previously with SipD, the peak perturbations were in the intermediate exchange on NMR timescale. While there were some peaks that mapped

onto the distal coiled-coil region, most of the perturbed peaks clustered at the mixed α-β region of IpaD$^{38-332}$. Also, majority of the affected residues from SipD and IpaD display either full conservation or similarity (charged, polar, hydrophobic) to each other and/or BipD. This suggests the presence of these residues at or near the tip-minor translocon binding interface.

To conclude, by using NMR, I investigated the interaction between the *Burkholderia* minor translocon protein BipC and the *Burkholderia* tip protein BipD as well as its homologs *Salmonella* SipD and *Shigella* IpaD. The outcome of this study suggests that BipC might be binding to the distal region likely at the α-β mixed region of the tip proteins. This study provides insight about the possible binding site of the minor translocon protein BipC on the tip protein BipD. The result of this study is significant as the binding site of the major translocon SipB has been shown to be located in this mixed α-β region of the tip protein SipD in *Salmonella* [26] and our finding suggests that BipC might also bind near the same interface. This would bring the two translocon proteins spatially in close proximity for interaction with one another, crucial for T3SS pore formation and function.

Additional experiments are needed to corroborate and validate the finding of this study regarding the tip-minor translocon interaction. Site-specific mutations introduced in the mixed α-β region of BipD and NMR or fluorescence based interaction studies with BipC would provide details of the tip-minor translocon interaction. Cell invasion assays for the wild type and the mutant tip proteins (mutations in the mixed α-β region) will also help establish any disruption in the T3SS assembly due to the introduced mutations in

that region. Other experiments could include assigning the NMR spectrum of BipD and BipC that will allow the direct identification of the amino acids at the interacting surface.

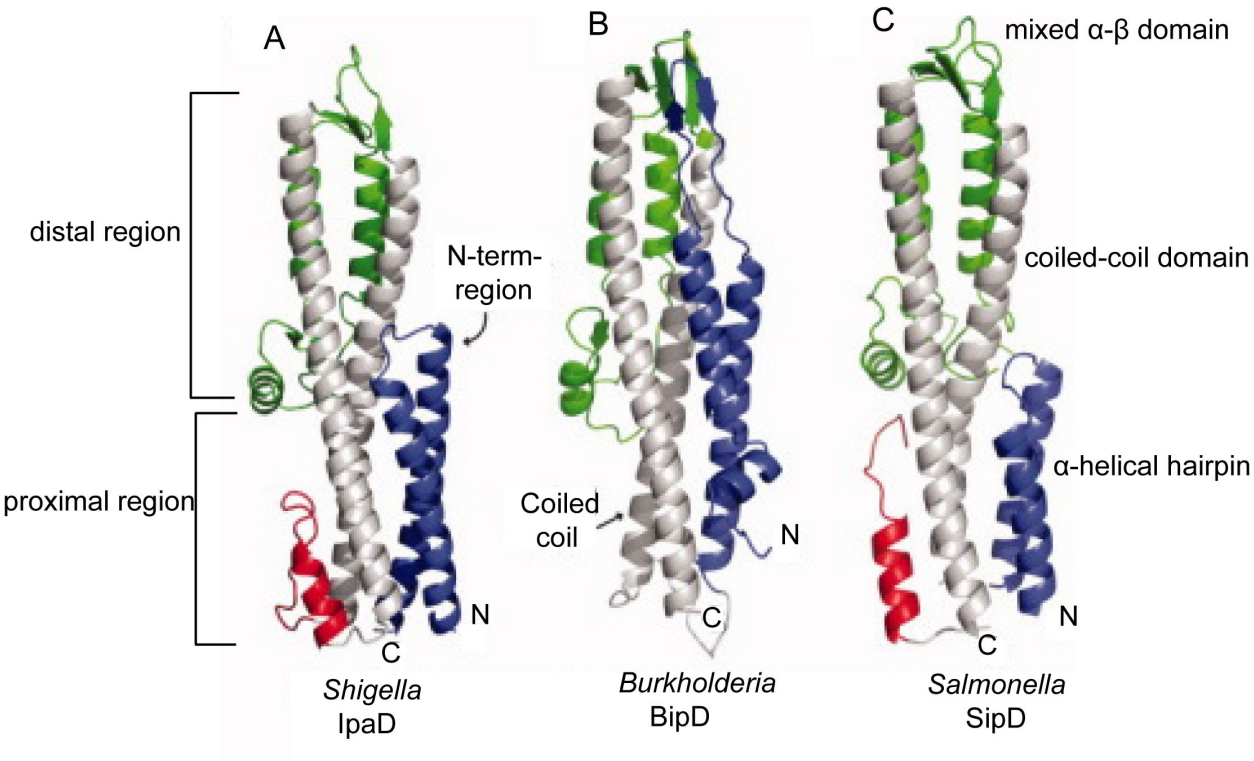

Figure 2-1. Comparison of the structures of the homologous tip poteins. **(A)** IpaD from *Shigella* **(B)** BipD from *Burkholderia* **(C)** SipD from *Salmonella.* All three tip proteins have an N-terminal α-helical hairpin (shown in blue), a central coiled-coil domain (shown in gray) and a mixed α-β domain (shown in green). The top half of the proteins is referred to as the distal region and faces opposite to the bacterial surface while the bottom half referred to as the proximal region faces the bacterial surface. The figure is adapted from Chatterjee et al [13].

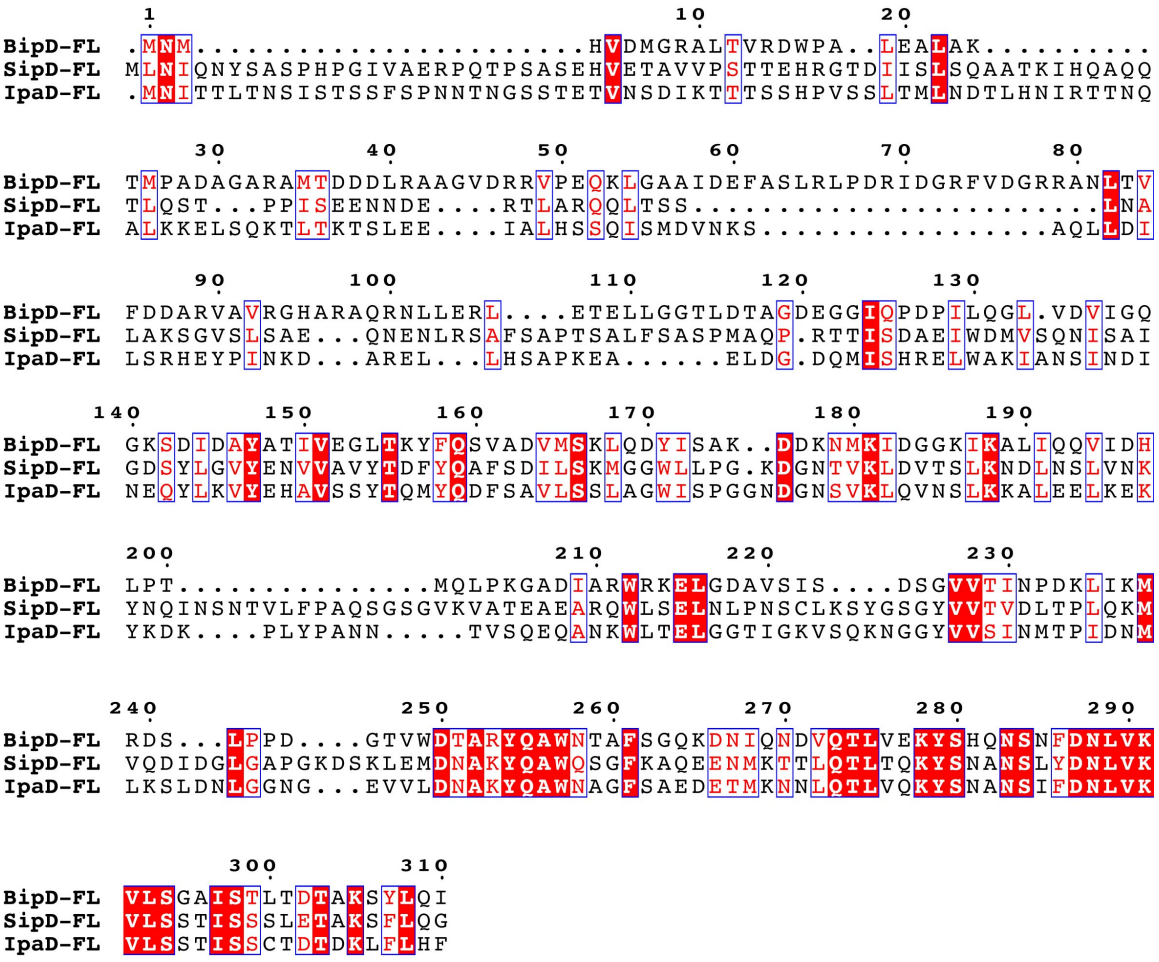

Figure 2-2. Primary sequence alignment of the homologous tip proteins BipD, SipD and IpaD from *Burkholderia*, *Salmonella* and *Shigella* respectively using Clustal Omega [21]. The figure was generated using ESPript 3.0 [24].

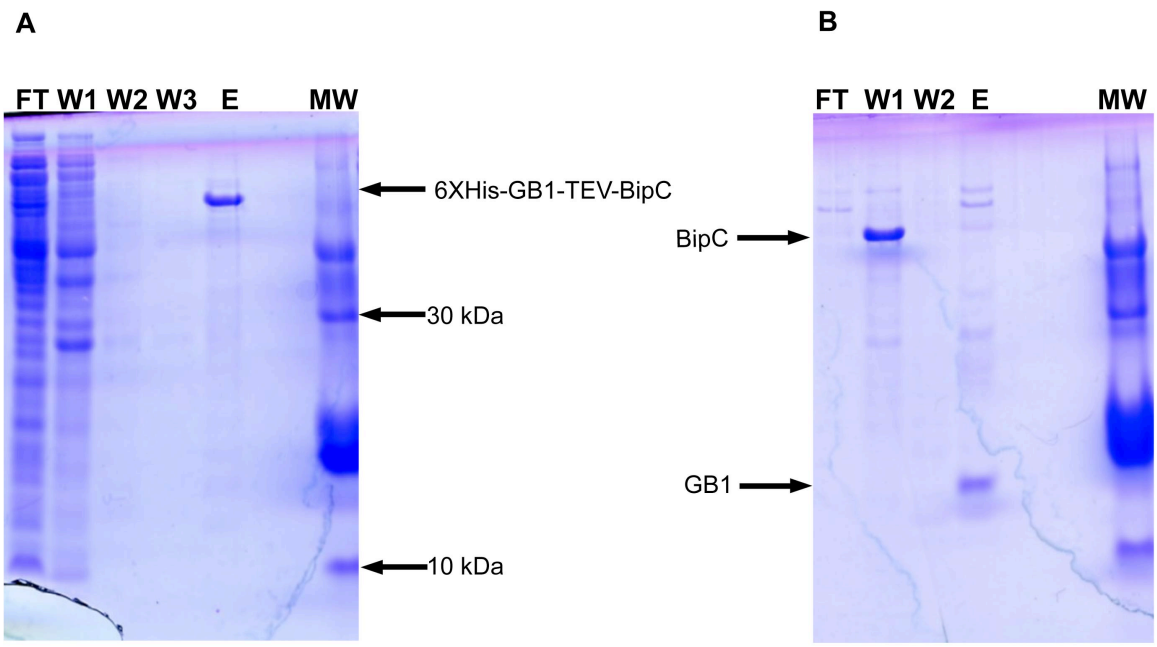

Figure 2-3. SDS-PAGE Gel of ^{15}N-BipC Purification. **(A)** Ni^{2+}- affinity chromatography purification of ^{15}N-BipC before TEV cleavage. The purified ^{15}N-BipC fused to His_6-GB1-TEV tag (~ 53.5kDa) is seen in the elution fraction. **(B)** Ni^{2+}- affinity chromatography purification of ^{15}N-BipC after TEV cleavage. The cleaved and purified ^{15}N-BipC (~ 44.5kDa) is seen in wash1 fraction while His_6-GB1-TEV tag (~ 9kDa) is seen in the elution fraction. (FT= flow through, W1= wash1, W2= wash2, W3= wash3, E= elution, MW=ladder).

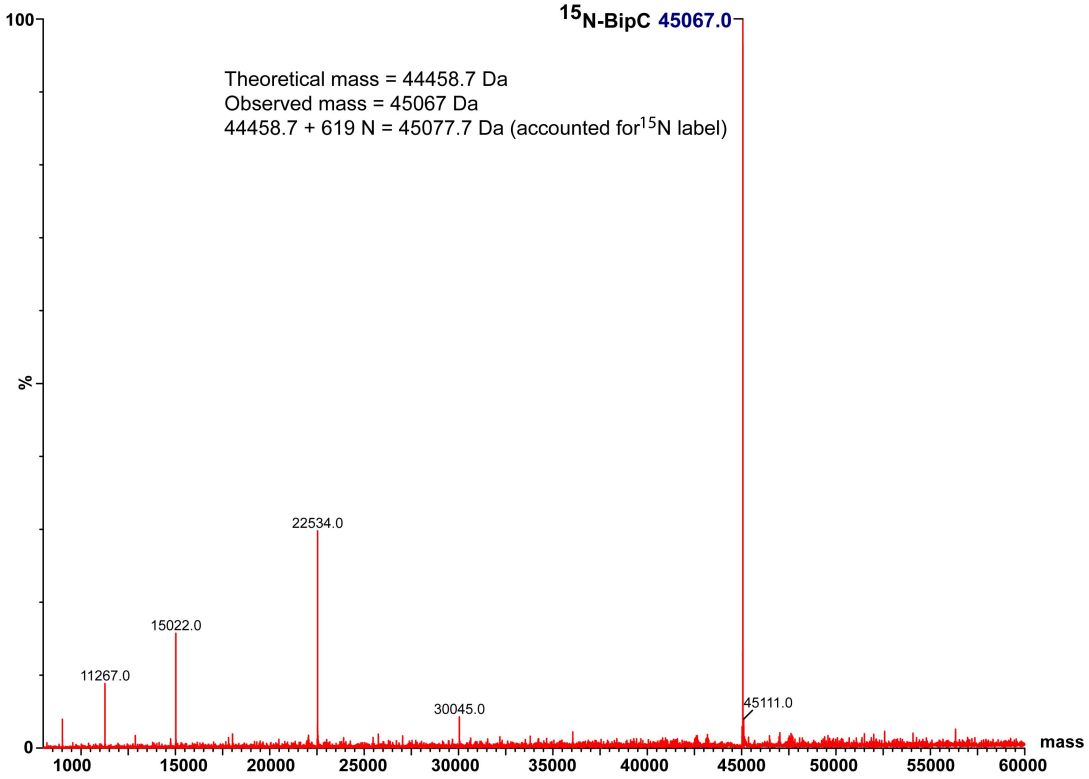

Figure 2-4. Electrospray ionization mass spectrometry to verify BipC expression. The theoretical and observed mass of BipC is shown in the figure to account for the difference in the mass due to ^{15}N labeling of BipC.

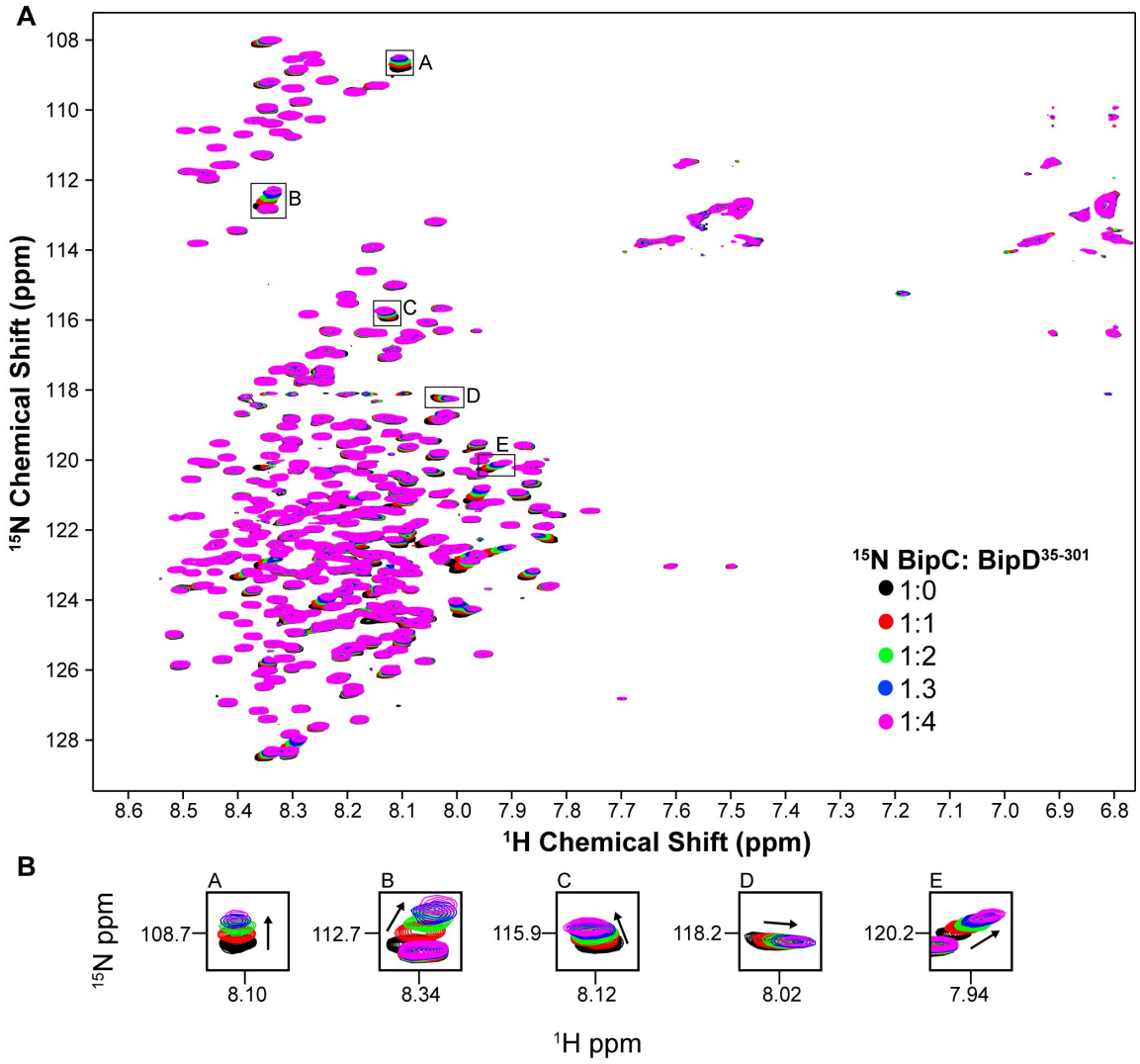

Figure 2-5. **(A)** Overlay of NMR titrations of ^{15}N-BipC with unlabeled BipD$^{35\text{-}301}$ at varying concentrations. **(B)** Expanded view of some peaks for clarity showing change in peak position.

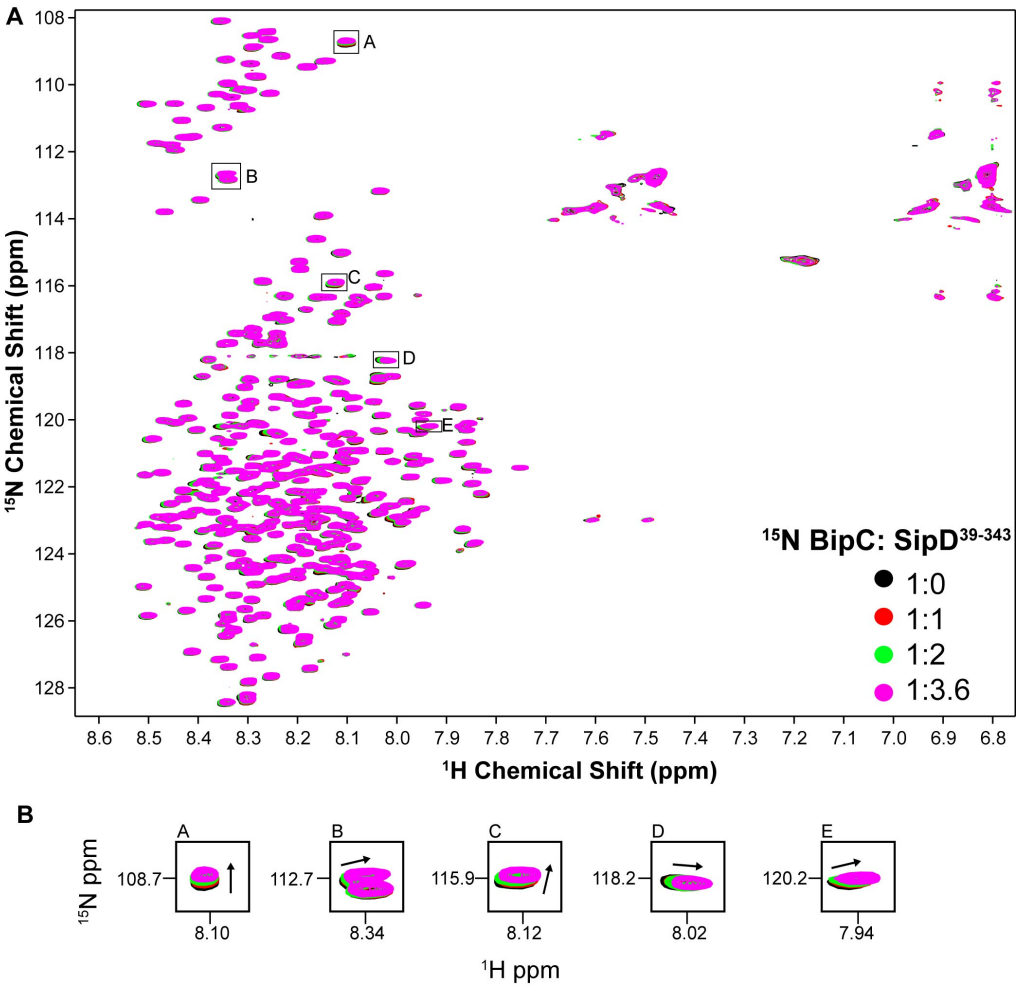

Figure 2-6. **(A)** Overlay of NMR titrations of ^{15}N-BipC with unlabeled SipD$^{39-343}$ at varying concentrations. **(B)** Expanded view of some peaks for clarity showing change in peak position.

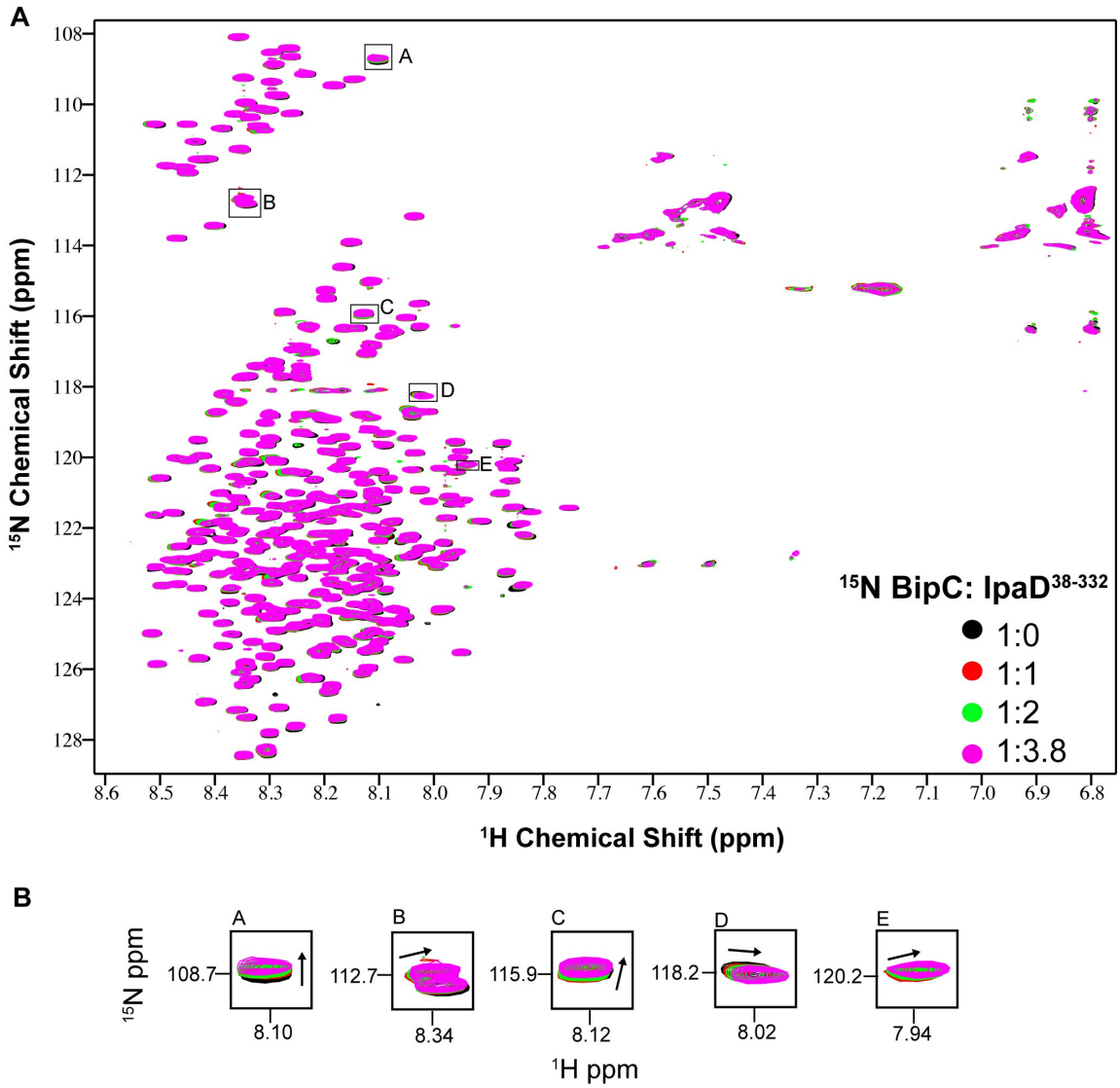

Figure 2-7. **(A)** Overlay of NMR titrations of ^{15}N-BipC with unlabeled IpaD$^{38-332}$ at varying concentrations. **(B)** Expanded view of some peaks for clarity showing change in peak position.

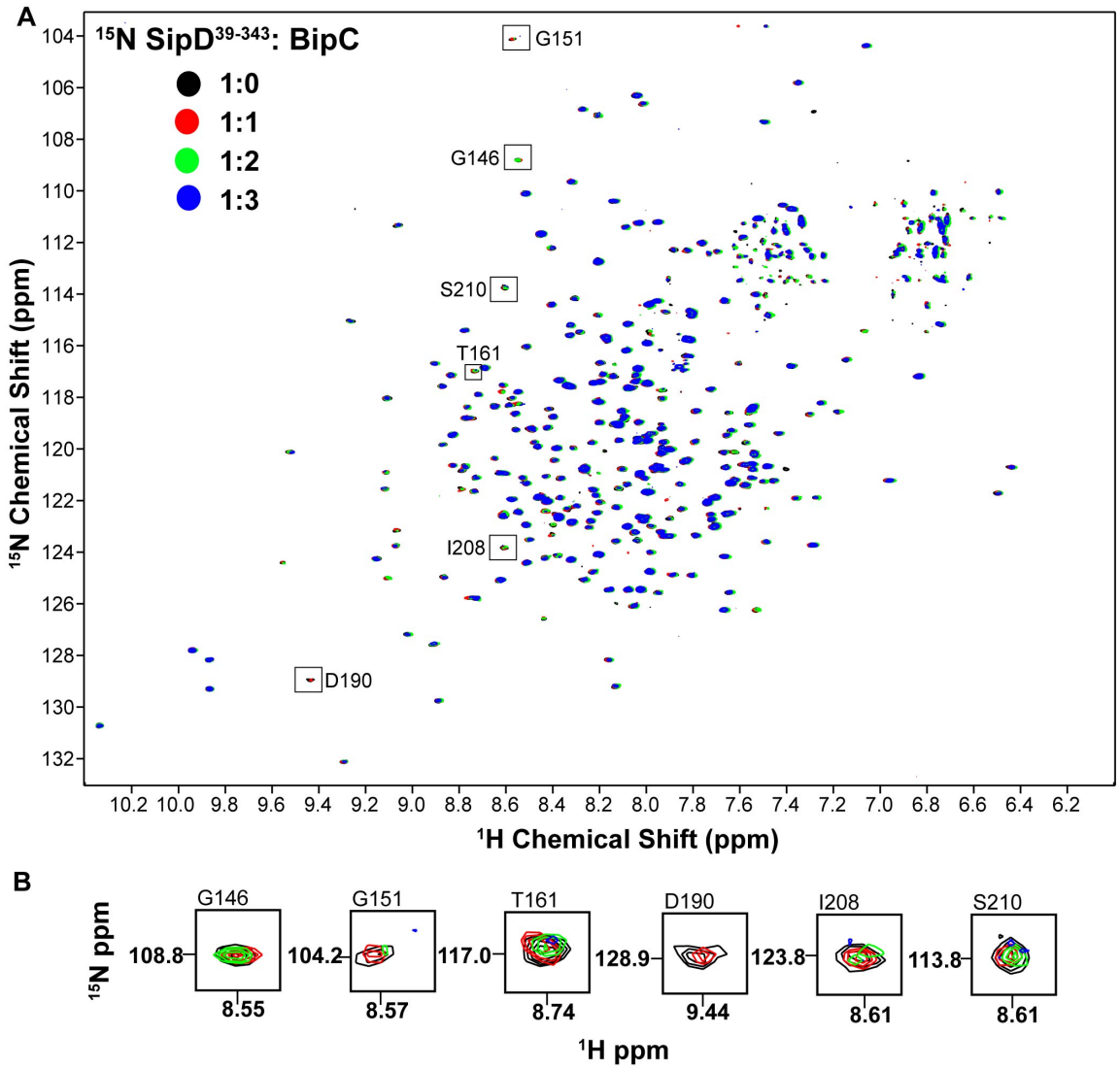

Figure 2-8. **(A)** Overlay of NMR titrations of ^{15}N-SipD$^{39-343}$ with unlabeled BipC at varying concentrations. **(B)** Expanded view of some peaks for clarity showing change in peak intensity.

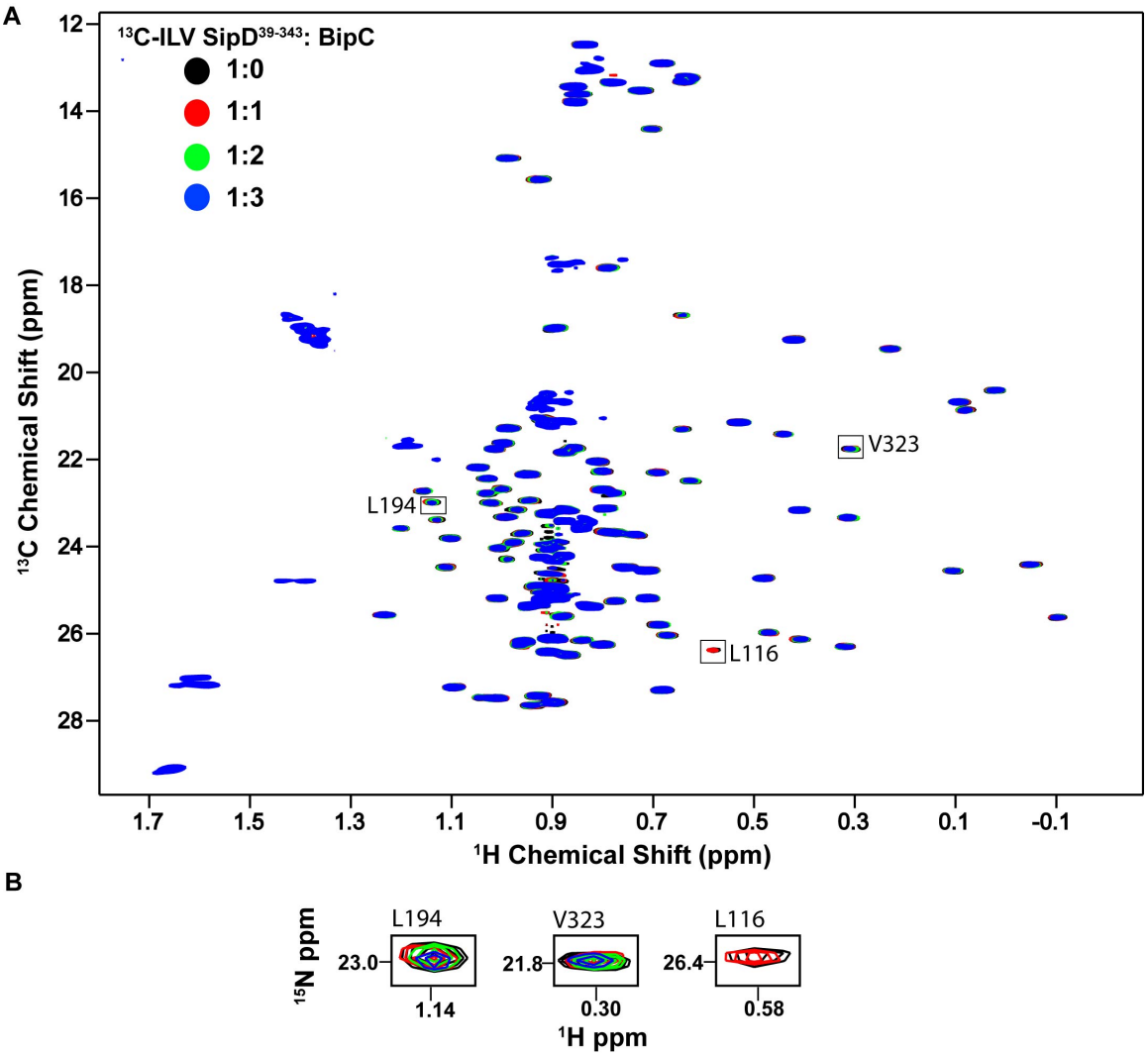

Figure 2-9. **(A)** Overlay of NMR titrations of ILV-SipD$^{39-343}$ with unlabeled BipC at varying concentrations. **(B)** Expanded view of some peaks for clarity showing change in peak intensity.

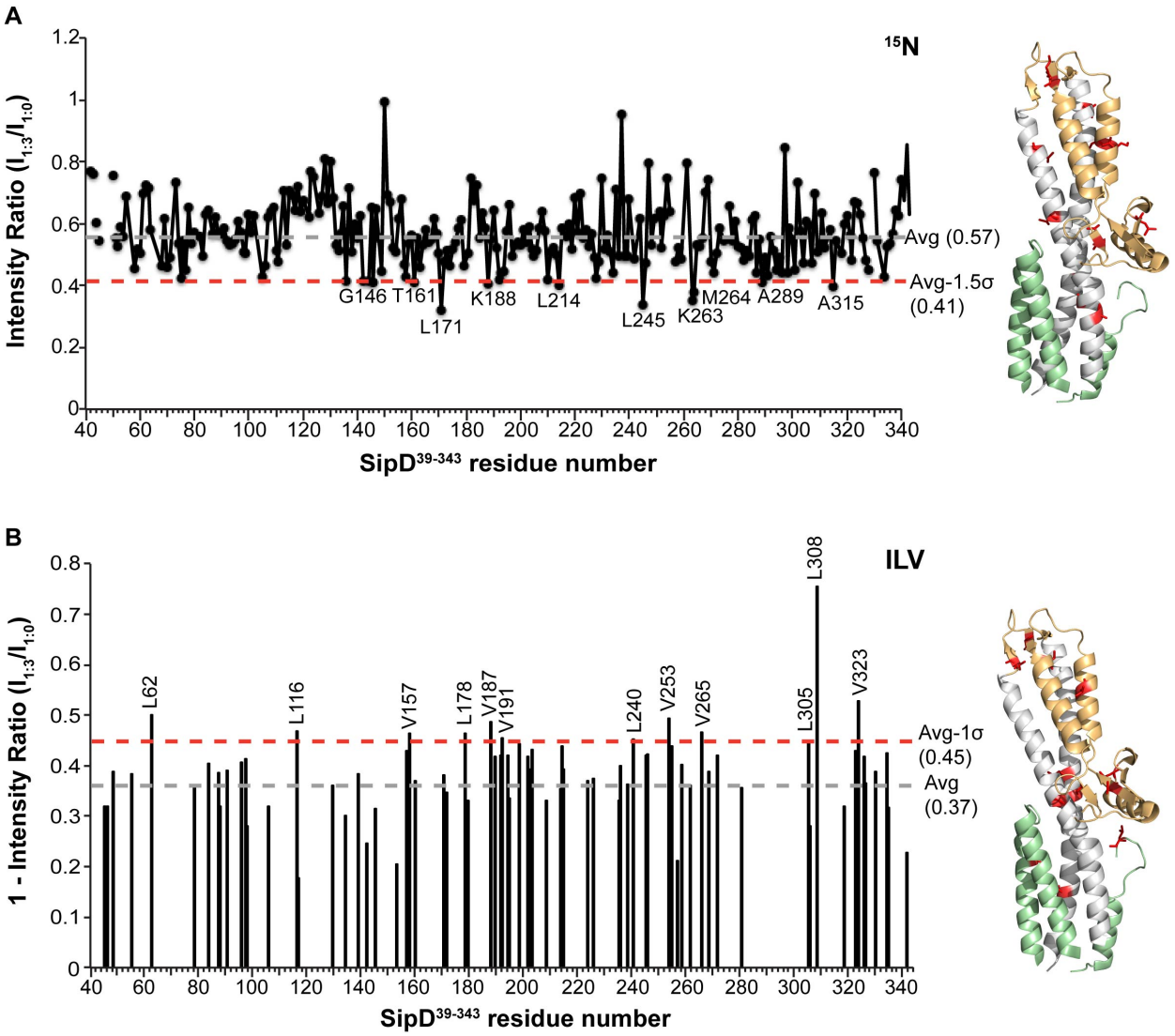

Figure 2-10. Quantification of peak intensity of ^{15}N and ILV-SipD$^{39-343}$ titrated with unlabeled BipC. **(A)** Peak intensity analysis of ^{15}N-SipD$^{39-343}$ with unlabeled BipC at the titration ratio of 1:3 compared to 1:0. **(B)** Peak intensity analysis of ILV-SipD$^{39-343}$ with unlabeled BipC at the titration ratio of 1:3 compared to 1:0. Gray line represents the average intensity value and the Red line represents the standard deviation subtracted from the average and was used as the threshold value.

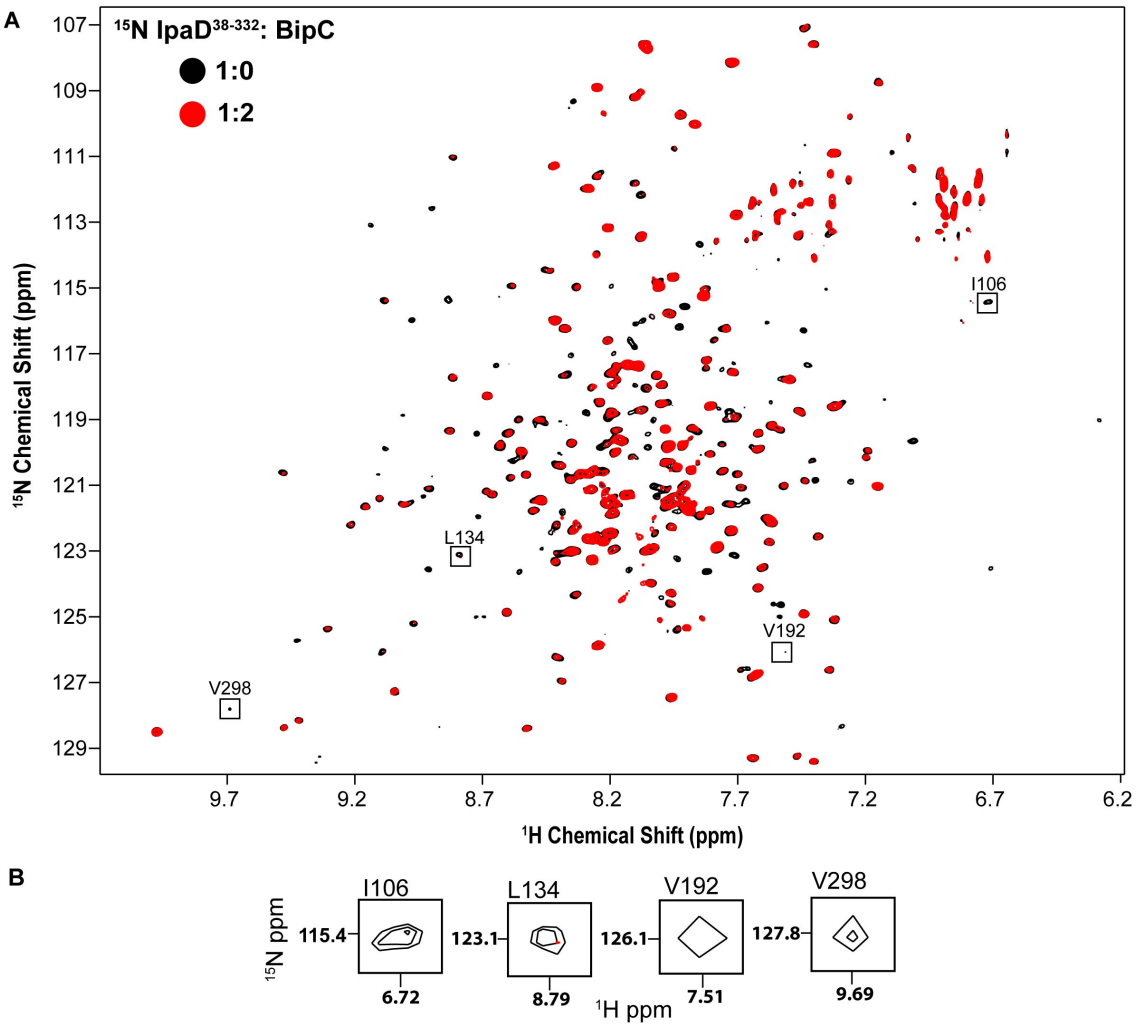

Figure 2-11. **(A)** Overlay of NMR titrations of ^{15}N-IpaD$^{38-332}$ with unlabeled BipC at varying concentrations. **(B)** Expanded view of some peaks for clarity showing change in peak intensity.

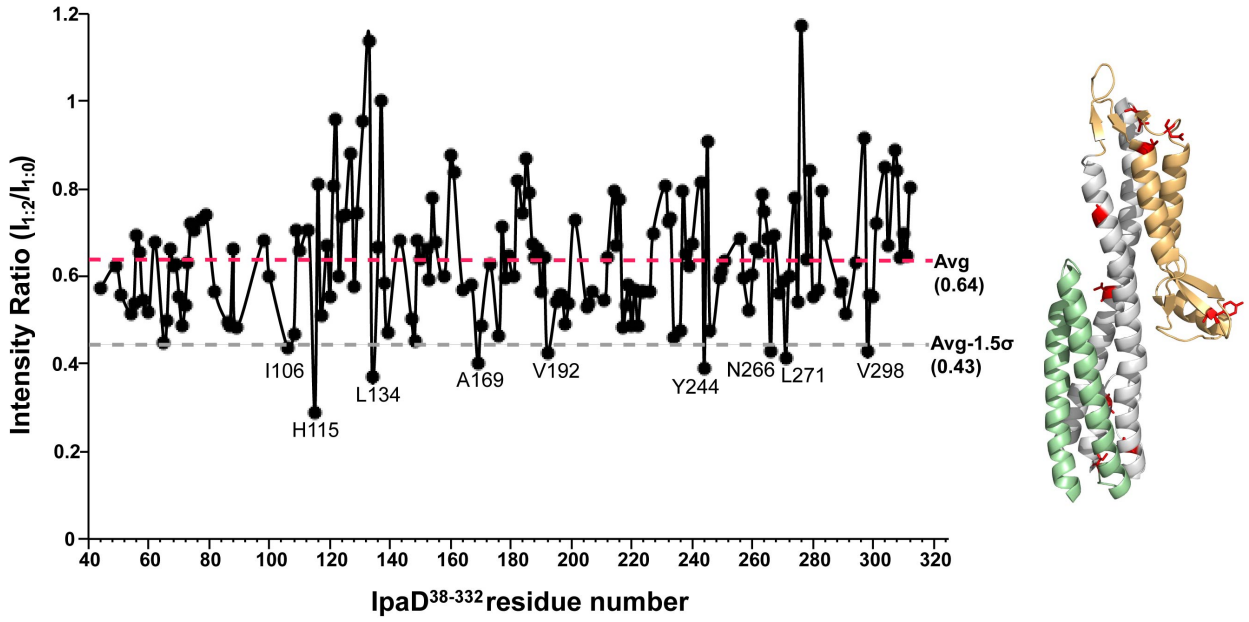

Figure 2-12. Quantification of peak intensity of ^{15}N-IpaD$^{38-332}$ with unlabeled BipC. Peak intensity analysis of ^{15}N-IpaD$^{38-332}$ with unlabeled BipC at the titration ratio of 1:2 compared to 1:0. Perturbed residues, in red are mapped on to the structure of IpaD. Gray line represents the average intensity value and the Red line represents the standard deviation subtracted from the average and was used as the threshold value.

2.5. References

[1] Sun, G. W., and Gan, Y. H. (2010) Unraveling type III secretion systems in the highly versatile Burkholderia pseudomallei, *Trends Microbiol 18*, 561-568.

[2] Limmathurotsakul, D., Golding, N., Dance, D. A., Messina, J. P., Pigott, D. M., Moyes, C. L., Rolim, D. B., Bertherat, E., Day, N. P., Peacock, S. J., and Hay, S. I. (2016) Predicted global distribution of Burkholderia pseudomallei and burden of melioidosis, *Nat Microbiol 1*.

[3] Wiersinga, W. J., Poll, T. V. d., White, N. J., Day, N. P., and Peacock, S. J. (2006) Melioidosis: insights into the pathogenicity of *Burkholderia pseudomallei*, *Nat. Rev. Microbiol. 4*, 272-282.

[4] Tian, D., and Zheng, T. (2014) Comparison and analysis of biological agent category lists based on biosafety and biodefense, *PLoS One 9*, e101163.

[5] Schweizer, H. P. (2012) Mechanisms of antibiotic resistance in Burkholderia pseudomallei: implications for treatment of melioidosis, *Future Microbiol 7*, 1389-1399.

[6] Galan, J. E., and Collmer, A. (1999) Type III secretion machines: bacterial devices for protein delivery into host cells, *Science 284*, 1322-1328.

[7] Moraes, T. F., Spreter, T., and Strynadka, N. C. (2008) Piecing together the type III injectisome of bacterial pathogens, *Curr Opin Struct Biol 18*, 258-266.

[8] Rainbow, L., Hart, C. A., and Winstanley, C. (2002) Distribution of type III secretion gene clusters in Burkholderia pseudomallei, B. thailandensis and B. mallei, *J Med Microbiol 51*, 374-384.

[9] Attree, O., and Attree, I. (2001) A second type III secretion system in Burkholderia pseudomallei: who is the real culprit?, *Microbiology (Society for General Microbiology) 147*, 3197-3199.

[10] Lee, Y. H., Chen, Y., Ouyang, X., and Gan, Y.-H. (2010) Identification of tomato plant as a novel host model for Burkholderia pseudomallei, *BMC Microbiology 10*, 28-28.

[11] Notti, R. Q., and Stebbins, C. E. (2016) The Structure and Function of Type III Secretion Systems, *Microbiol Spectr 4*.

[12] McShan, A. C. (2015) The Bacterial Type III Secretion System as a Target for Developing New Antibiotics, *Chemical biology & drug design 85*, 30-42.

[13] Chatterjee, S., Zhong, D., Nordhues, B. A., Battaile, K. P., Lovell, S., and De Guzman, R. N. (2011) The crystal structures of the Salmonella type III secretion system tip protein SipD in complex with deoxycholate and chenodeoxycholate, *Protein Sci 20*, 75-86.

[14] Sievers, F., Wilm, A., Dineen, D., Gibson, T. J., Karplus, K., Li, W., Lopez, R., McWilliam, H., Remmert, M., Söding, J., Thompson, J. D., and Higgins, D. G. (2011) Fast, scalable generation of high- quality protein multiple sequence alignments using Clustal Omega, *Molecular Systems Biology 7*, n/a-n/a.

[15] Li, W., Cowley, A., Uludag, M., Gur, T., McWilliam, H., Squizzato, S., Park, Y. M., Buso, N., and Lopez, R. (2015) The EMBL-EBI bioinformatics web and programmatic tools framework, *Nucleic Acids Res 43*, W580-584.

[16] Robert, X., and Gouet, P. (2014) Deciphering key features in protein structures with the new ENDscript server, *Nucleic Acids Research 42*, W320-W324.

[17] Kaur, K., Chatterjee, S., and De Guzman, R. N. (2016) Characterization of the Shigella and Salmonella Type III Secretion System Tip-Translocon Protein-Protein Interaction by Paramagnetic Relaxation Enhancement, *Chembiochem 17*, 745-752.

[18] Zhou, P., and Wagner, G. (2010) Overcoming the solubility limit with solubility-enhancement tags: successful applications in biomolecular NMR studies, *J Biomol NMR 46*, 23-31.

[19] McShan, A. C., Anbanandam, A., Patnaik, S., and De Guzman, R. N. (2016) Characterization of the Binding of Hydroxyindole, Indoleacetic acid, and Morpholinoaniline to the Salmonella Type III Secretion System Proteins SipD and SipB, *ChemMedChem 11*, 963-971.

[20] Geisbrecht, B. V., Bouyain, S., and Pop, M. (2006) An optimized system for expression and purification of secreted bacterial proteins, *Protein Expr Purif 46*, 23-32.

[21] Leahy, D. J., Dann, C. E., 3rd, Longo, P., Perman, B., and Ramyar, K. X. (2000) A mammalian expression vector for expression and purification of secreted proteins for structural studies, *Protein Expr Purif 20*, 500-506.

[22] Delaglio, F., Grzesiek, S., Vuister, G. W., Zhu, G., Pfeifer, J., and Bax, A. (1995) NMRPipe: a multidimensional spectral processing system based on UNIX pipes, *J Biomol NMR 6*, 277-293.

[23] Johnson, B. A. (2004) Using NMRView to visualize and analyze the NMR spectra of macromolecules, *Methods Mol Biol 278*, 313-352.

[24] Czisch, M., and Boelens, R. (1998) Sensitivity enhancement in the TROSY experiment, *J Magn Reson 134*, 158-160.

[25] Wang, Y., Nordhues, B. A., Zhong, D., and De Guzman, R. N. (2010) NMR characterization of the interaction of the Salmonella type III secretion system protein SipD and bile salts, *Biochemistry 49*, 4220-4226.

[26] McShan, A. C., Kaur, K., Chatterjee, S., Knight, K. M., and De Guzman, R. N. (2016) NMR identification of the binding surfaces involved in the Salmonella and Shigella Type III secretion tip-translocon protein-protein interactions, *Proteins 84*, 1097-1107.

[27] Dickenson, N. E., Zhang, L., Epler, C. R., Adam, P. R., Picking, W. L., and Picking, W. D. (2011) Conformational changes in IpaD from Shigella flexneri upon binding bile salts provide insight into the second step of type III secretion, *Biochemistry 50*, 172-180.

Chapter 3: Conformational and structural changes of *Burkholderia* minor translocon protein BipC in the presence of membrane mimetic detergents

3.1. Introduction

The type III secretion system (T3SS) plays an important role in the pathogenesis of many pathogenic Gram-negative bacteria [1]. The T3SS is a syringe-like apparatus assembled from over 20 different proteins [2, 3] (Figure 1-1 and 1-2). There are two translocon proteins called the major and the minor translocon proteins based on their respective molecular weights, that are essential for the formation of the transmembrane channel allowing the export of effector molecules (Figure 1-2). The minor translocon proteins of the type III secretion system are transmembrane proteins that are mostly helical with a single predicted transmembrane domain [4] (Figure 3-1 and 3-2).

The minor translocon proteins from *Salmonella* and *Shigella* have been shown to interact and insert into host membrane and liposomes and are vital for the export of virulence effector molecules into the host [5, 6, 7]. The minor translocon protein from *Burkholderia*, BipC, has not been well characterized and the information on its interaction with membrane is unknown and is the subject of study in this chapter.

BipC is the minor translocon protein of *Burkholderia pseudomallei* [8]. A BipC construct has been successfully cloned, expressed and purified in our lab (Dr. Supratim Dey). Secondary structure prediction using the Network Protein Sequence Analysis (NPS@) server, predicts BipC to be extensively helical [9] (Figure 3-2). The NMR study of the BipC construct shows a narrow dispersion of < 1 ppm (Figure 2-5). This narrow dispersion is consistent with its predicted extensive α-helical structure, as mostly α-

helical proteins generally display narrow ^{1}H chemical shift dispersion due to the exposure of the amino acids in the helices to similar local chemical environment [10]. On the other hand, the secondary structural analysis using CD spectroscopy herein shows BipC to be mostly random coil with partial α-helix that is in contradiction with its predicted vastly helical structure.

Thus, in this chapter I looked at the conformational and structural changes in the *Burkholderia* minor translocon protein BipC in the presence of different membrane mimetic detergents, dodecylphosphocholine (DPC), and lyso-myristoylphosphatidylglycerol (LMPG) by NMR and CD spectroscopy. The above two detergents were selected for this study because they resemble the structure of the phospholipids in the lipid bilayers, retain and maintain protein structure and function, and yield good NMR spectra [10, 11]. Thus, both DPC and LMPG have been widely used as suitable membrane mimicking detergents of choice for structural and functional studies of membrane proteins [10, 11, 12, 13].

3.2. Experimental Section

3.2.1. Overexpression and purification of ^{15}N-labeled BipC

Uniformly ^{15}N-labeled full length BipC was expressed and purified as described in Chapter 2. Briefly, BipC construct with an N-terminal His_6-GB1 and TEV protease tag was overexpressed in *E.coli* BL21-CodonPlus (DE3)-RIPL strain. The bacterial cells were then harvested by centrifugation, lysed by sonication and the protein was purified by nickel affinity chromatography twice, the second time following the cleavage of the

His_6-GB1 tag. ^{15}N-labeled BipC fractions were pooled together, concentrated using a commercial Amicon 3K filter unit, and protein concentration estimated by Bradford assay.

3.2.2. Preparation of detergent stocks

The stock solutions were prepared for DPC and LMPG in NMR buffer (20 mM phosphate, 100 mM NaCl, pH 6.8) for NMR titration experiments and in water for CD spectroscopy experiments. The stock detergent solutions were solubilized by repeated freeze thaw cycles in liquid nitrogen or -80 °C until the solution became clear after which the stocks were kept at 4 °C for long-term storage.

3.2.3. Secondary structure and TM prediction

The network protein sequence analysis (NPS@) Web server was employed to estimate the secondary structure of BipC [9]. The hydrophobicity plots of *Burkholderia* BipC and its homologs *Salmonella* SipC and *Shigella* IpaC were created using the Dense Alignment Surface (DAS) transmembrane prediction server to predict the transmembrane (TM) domain of the minor translocon proteins [14]. Clustal Omega online server was used to align the protein sequences [15] and the alignment results were processed and an alignment figure generated using ESPript 3.0 [16].

3.2.4. Circular Dichroism experiments

Data were acquired using a Jasco J-815 spectropolarimeter. All samples were prepared in water to a final volume of 3 mL. The protein concentration used was

0.05mg/mL titrated with increasing concentrations of the DPC and LMPG ranging from below to above their respective CMCs of 1.1 mM and 0.3 mM. All CD spectra were acquired in triplicate in a quartz cuvette with a path length of 10 cm and scanning speed of 50 nm/min. Dichroweb server was used to estimate the secondary structure of BipC using the CDSSTR algorithm [17, 18].

3.2.5. NMR titration experiments

The titration experiments were carried out with ^{15}N-labeled BipC titrated with different concentrations of the detergents. The titration concentrations used for DPC were below and above the CMC of 1.1mM of DPC, and at and above the CMC of 0.3mM of LMPG [19]. All NMR data were collected using a Bruker Advance 800 MHz spectrometer equipped with a cryogenic triple resonance probe. The acquisition parameters were 40 scans, 2048 ^{1}H complex points, and 400 ^{15}N complex points. The ^{15}N sweep width was 30 ppm centered at 118 ppm and the ^{1}H sweep width was 18 ppm centered at 4.7 ppm. The NMR data were processed and analyzed by using NMRPipe [20] and NMRView [21].

3.3. Results

3.3.1. Secondary structure and TM prediction

The NPS@ Web server predicted BipC to have extensive helices [9] (Figure 3-2). The DAS TM prediction [14] server did not show a clear transmembrane region for BipC above the strict cut off value (Figure 3-3). On the other hand, BipC homologs

Salmonella SipC and *Shigella* IpaC, both showed a well predicted transmembrane region above the strict cut off value (Figure 3-3). The discrepancy in the TM prediction was investigated further by aligning the sequences of BipC, SipC and IpaC using Clustal Omega server [15]. The alignment result showed the presence of a combination of charged and polar residues in BipC in the predicted transmembrane region for its homologs SipC and IpaC, which might be why prediction servers did not yield a well predicted TM region for BipC (Figure 3-4).

3.3.2. Monitoring secondary structural changes of BipC by Circular Dichroism

The CD analysis of BipC construct used in this study showed a predominantly random coil conformation with some helicity (Figure 3-5 and 3-6). IpaC, the minor translocon protein from *Shigella* also shows a similar CD spectrum [6]. The titration experiments by CD spectroscopy in this chapter showed that BipC gained in α-helicity in the presence of increasing concentrations of both detergents, DPC and LMPG.

The BipC construct in the absence of DPC showed a minimum at ~200 nm and a slight minimum at ~222 nm which is characteristic of a protein that is mostly random coil with partial helical content (Figure 3-5). As BipC was titrated with increasing concentrations of DPC, there was a significant shift in its secondary structure from random coil to mostly α-helical evident by the minima shift from ~200 nm towards ~208 nm [22]. This structural change was more pronounced as the DPC concentration reached above its CMC value suggesting BipC interaction and possible insertion into DPC micelles. The molar ellipticity ratio ($\theta_{222}/\theta_{208}$) is another parameter that indicates interhelical contacts [23]. Extensive inter-helical contacts as in coiled-coil show a $\theta_{222}/\theta_{208}$

ratio of 1.0 and above while isolated helices show a $\theta_{222}/\theta_{208}$ of ~0.8 [23]. The titration of BipC with DPC increased its $\theta_{222}/\theta_{208}$ ratio from ~0.55 to ~0.69 indicative of absence of any extensive helical contacts as in coiled-coil. The secondary structure estimation from the CD data using CDSSTR algorithm by Dichroweb server showed a significant increase in helix content of BipC up to 5mM DPC and a slight decrease thereafter (Table 2A**)**.

BipC titration experiments with LMPG also corroborate the results obtained with DPC. There was a marked shift in the CD spectrum of BipC in the presence of LMPG as seen from the shift in the minima from ~ 200 nm towards ~208 nm [22]. The $\theta_{222}/\theta_{208}$ ratio increased from ~0.55 to ~0.78 signifying lack of inter-helical contacts and probable isolated helices. The one observation that was different from the DPC experiment was that the structural transition was apparent even at a concentration that was below the CMC of 0.3 mM of LMPG (Figure 3-6). The structural change evident from the CD spectra was also supported by an increase in the helical content of BipC with increasing LMPG concentration as estimated by Dichroweb server using CDSSTR algorithm (Table 2B).

3.3.3. BipC interaction with detergents by NMR

To study the interaction of BipC with the detergents, uniformly ^{15}N-labeled BipC was titrated with two detergents, DPC and LMPG and probed by NMR. The NMR spectrum of ^{15}N-labeled BipC in the presence of 0.5 mM DPC, which is below the CMC of 1.1 mM of DPC, does not show major changes in peak chemical shift values (Figure 3-7 and 3-8). As I titrated ^{15}N-labeled BipC with 25 mM DPC, which is above the CMC

of DPC, a significant peak broadening as well as peak loss was observed (Figure 3-7 and 3-8). About 75 peaks out of approximately 302 ^{15}N-BipC amide peaks showed large deviation in peak positions in the presence of DPC above its CMC signifying potential conformational changes in BipC (Figure 3-8).

In a similar manner, the effect of LMPG on ^{15}N-labeled BipC was studied. ^{15}N-labeled BipC showed no significant peak perturbation at the CMC concentration of 0.3 mM LMPG while it displayed substantial chemical shift perturbation evident by deviation in peak position as well as reduced peak intensities of several amide peaks leading to significant peak loss at a titration concentration above the CMC of LMPG (Figure 3-9 and 3-10). As seen with DPC, over 70 peaks out of approximately 302 ^{15}N-BipC amide peaks showed large change in peak positions and or intensity in the presence of LMPG above its CMC indicating potential conformational changes in BipC (Figure 3-10).

3.4. Discussion

BipC is the *Burkholderia* minor translocon protein but it lacks a clearly predicted transmembrane region as opposed to its homologs *Salmonella* SipC and *Shigella* IpaC using TM prediction servers (Figure 3-3). When the primary sequence of BipC was aligned, and compared to SipC and IpaC, it was found that BipC harbors charged and polar residues in the TM region predicted for SipC and IpaC (Figure 3-4). The overall number of charged amino acids in BipC is also much larger than either SipC or IpaC. This could also explain why BipC is expressed and purified as a soluble protein whereas SipC and IpaC are insoluble in the absence of their chaperones.

Secondary structure prediction using NPS@ Web server predicted BipC to be vastly helical [9] (Figure 3-2) whereas the CD spectrum of BipC construct used in this study showed a predominantly random coil conformation with some helicity (Figure 3-5 and 3-6). Similar CD spectrum has been reported for IpaC [6]. To investigate this disparity, I employed titration experiments to study the secondary structural changes of BipC in the absence and presence of varying concentrations of DPC and LMPG detergents by CD spectroscopy. The CD data clearly show a secondary structural transition from a random coil to a helical protein (Figure 3-5 and 3-6). The secondary structure estimation by the CDSSTR algorithm using the Dichroweb server also showed increased α-helicity for BipC in detergent micelles (Table 3-2).

The NMR study also suggests interaction of BipC with the detergents. The significant peak loss observed in the presence of the detergents above the CMC concentration indicates probable insertion of BipC into the detergent micelles. As BipC inserts into the detergent micelles, its tumbling rate might be reduced which leads to the peak broadening and peak loss observed in the spectra (Figure 3-7 to Figure 3-10). This difference in the NMR spectrum of BipC and extensive pek perturbation shown by a majority of the amide peaks in the presence of detergents demonstrates a change in the conformation and structure of BipC.

In summary, the biophysical study carried out herein showed a major conformational and structural change in BipC when titrated with membrane mimetic detergents. This has added to the knowledge that is available about the structural assembly of T3SS. As such, it will be interesting to investigate the implication of these

structural changes in BipC in its ability to interact with its binding partners and form a functional T3SS.

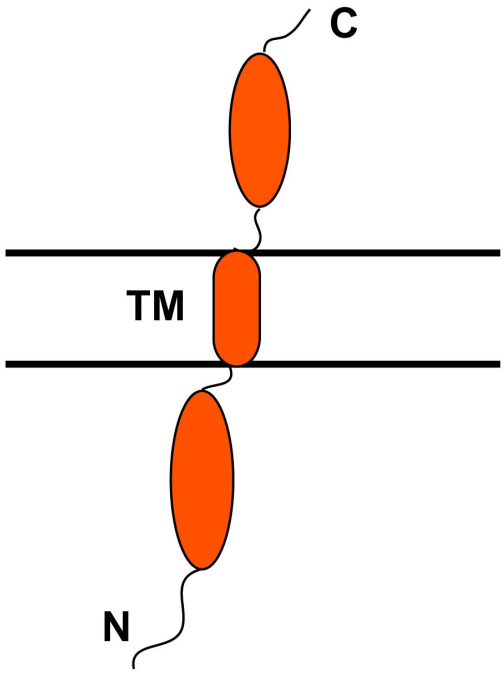

Figure 3-1. A cartoon representation of the T3SS minor translocon protein showing the single predicted transmembrane (TM) region.

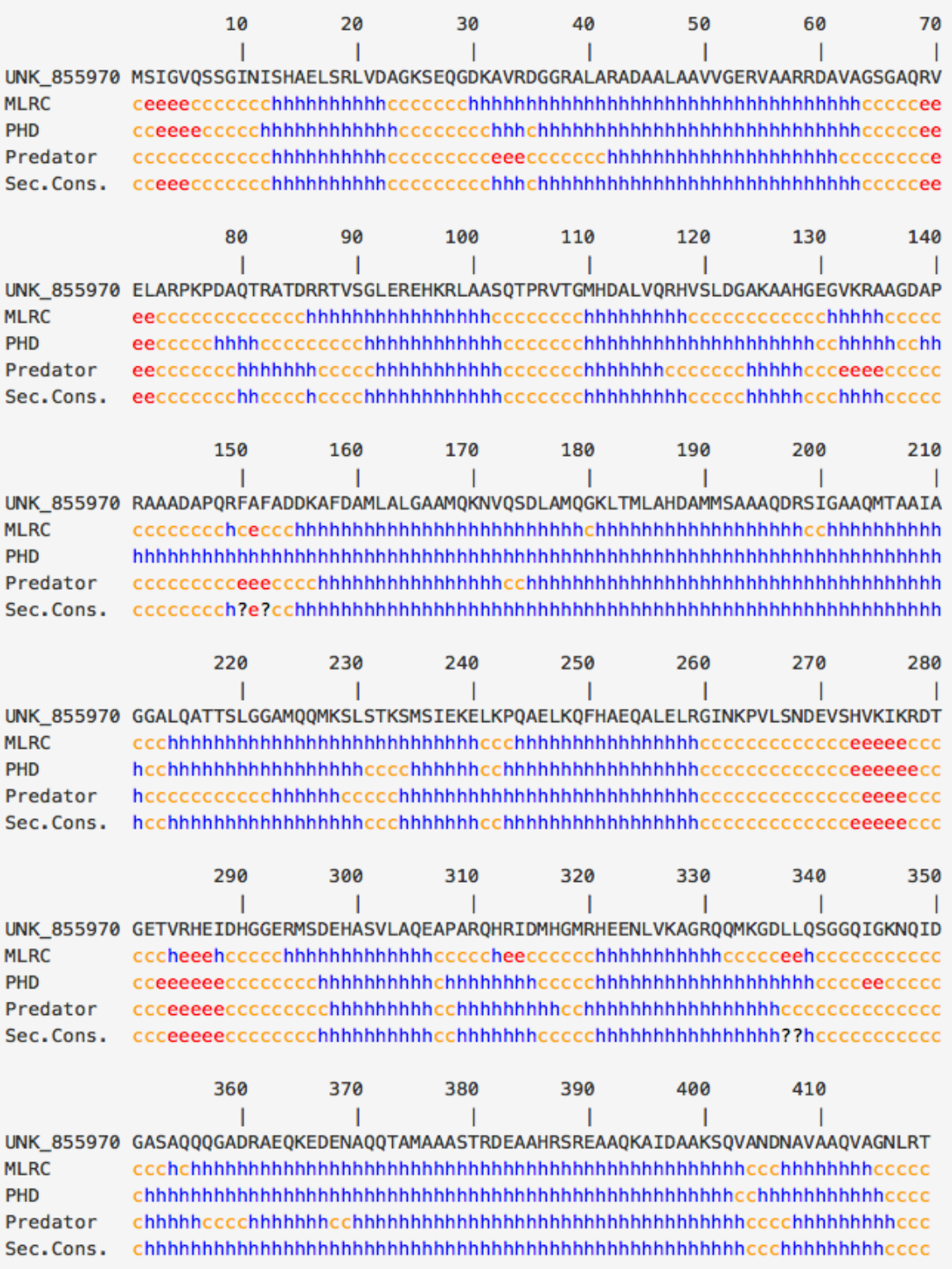

Figure 3-2. Secondary structure prediction of *Burkholderia* minor translocon protein BipC using the Network Protein Sequence Analysis (NPS@) Web server [9].

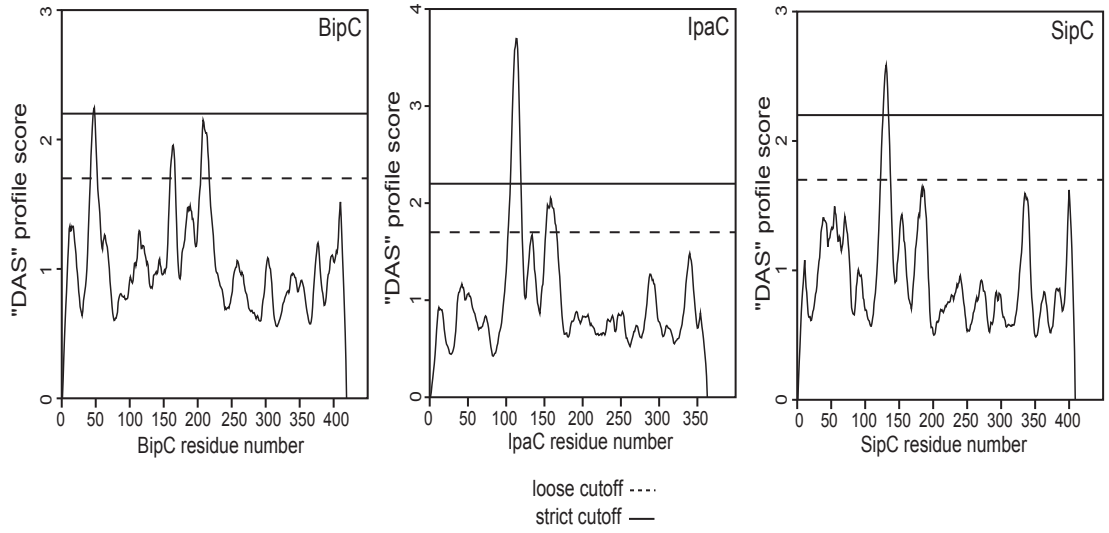

Figure 3-3. Comparison of the predicted hydropathy plots for the minor transocon proteins *Burkholderia* BipC, *Shigella* IpaC and *Salmonella* SipC using DAS Prediction Server [14].

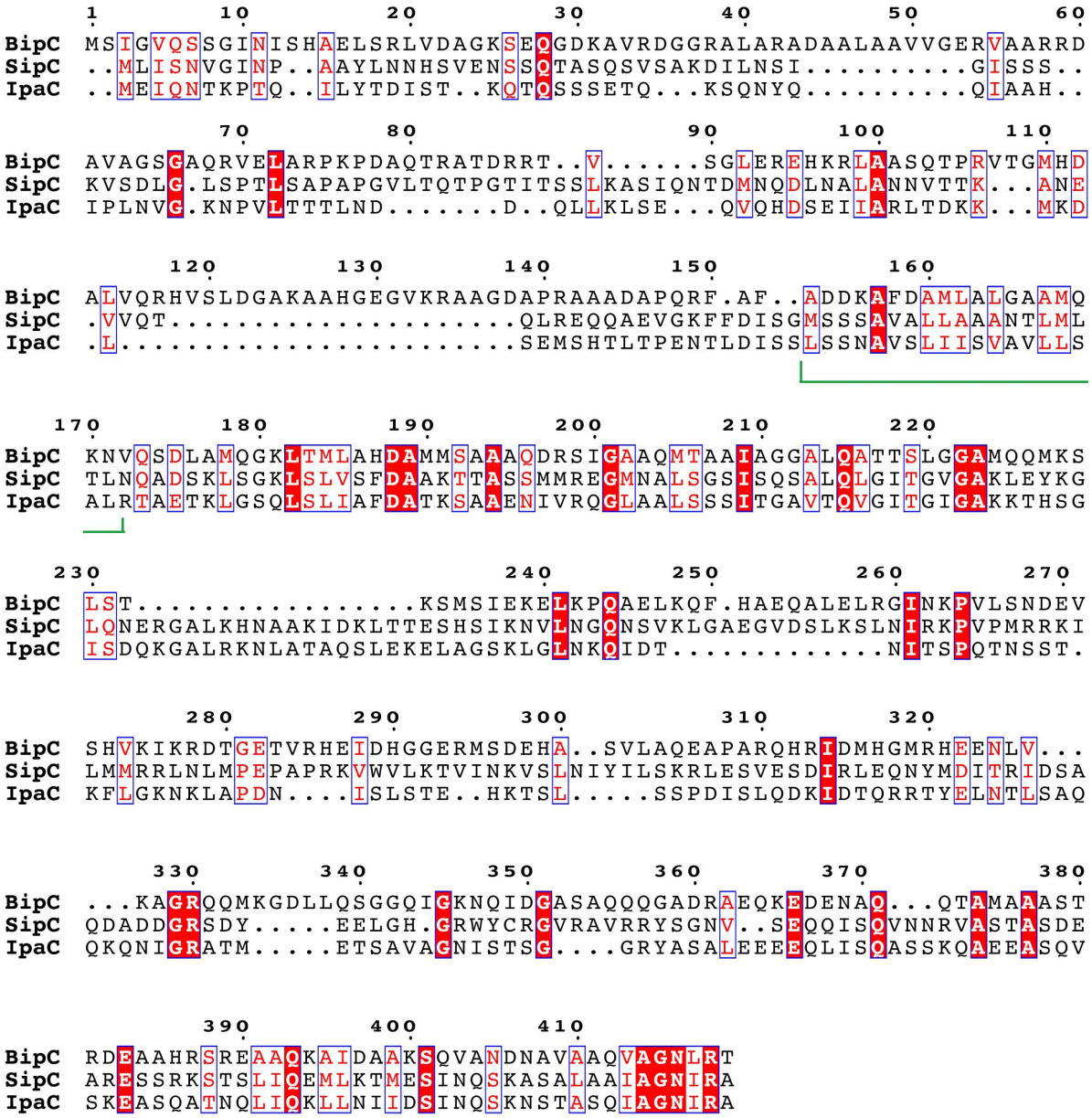

Figure 3-4. Primary sequence alignment of minor translocons BipC, SipC and IpaC from *Burkholderia*, *Salmonella* and *Shigella* respectively. The green bracket highlights the predicted TM region for SipC and IpaC showing BipC harboring charged and polar residues in that region. Sequences were aligned using CLustal Omega [15] and the figure generated using ESPript 3.0 [16].

A

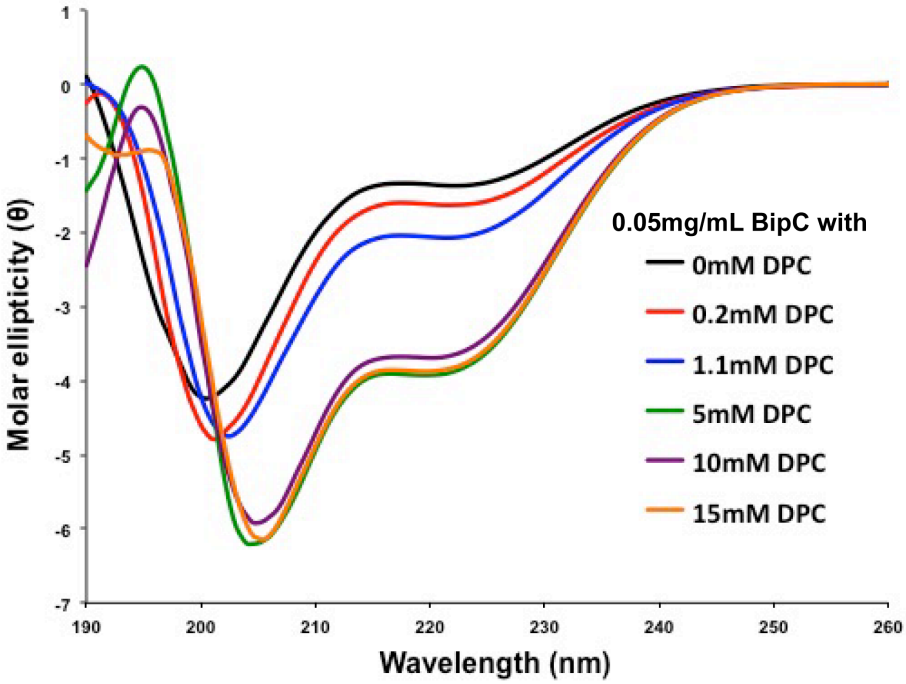

B

DPC conc.	Θ 222/208
0 mM	0.55
0.2 mM	0.54
1.1 mM	0.60
5 mM	0.69
10 mM	0.68
15 mM	0.69

Figure 3-5. Circular Dichroism analysis of BipC in DPC. Each titration ratio is color coded as shown in legend. **(A)** CD spectra of BipC titrated with increasing concentrations of DPC. **(B)** The molar ellipticity ratio of $\theta_{222}/\theta_{208}$ for the titration of BipC with DPC.

A

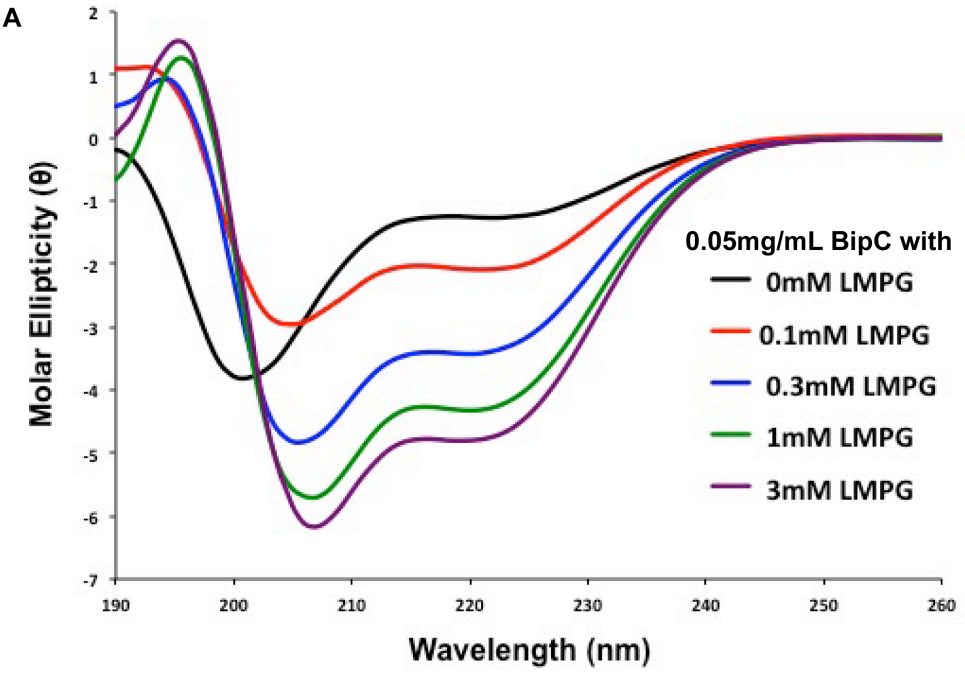

B

LMPG conc.	Θ 222/208
0 mM	0.55
0.1 mM	0.77
0.3 mM	0.74
1 mM	0.76
3 mM	0.78

Figure 3-6. Circular Dichroism analysis of BipC in LMPG. Each titration ratio is color coded as shown in legend. **(A)** CD spectra of BipC titrated with increasing concentrations of LMPG. **(B)** The molar ellipticity ratio of $\theta_{222}/\theta_{208}$ for the titration of BipC with LMPG.

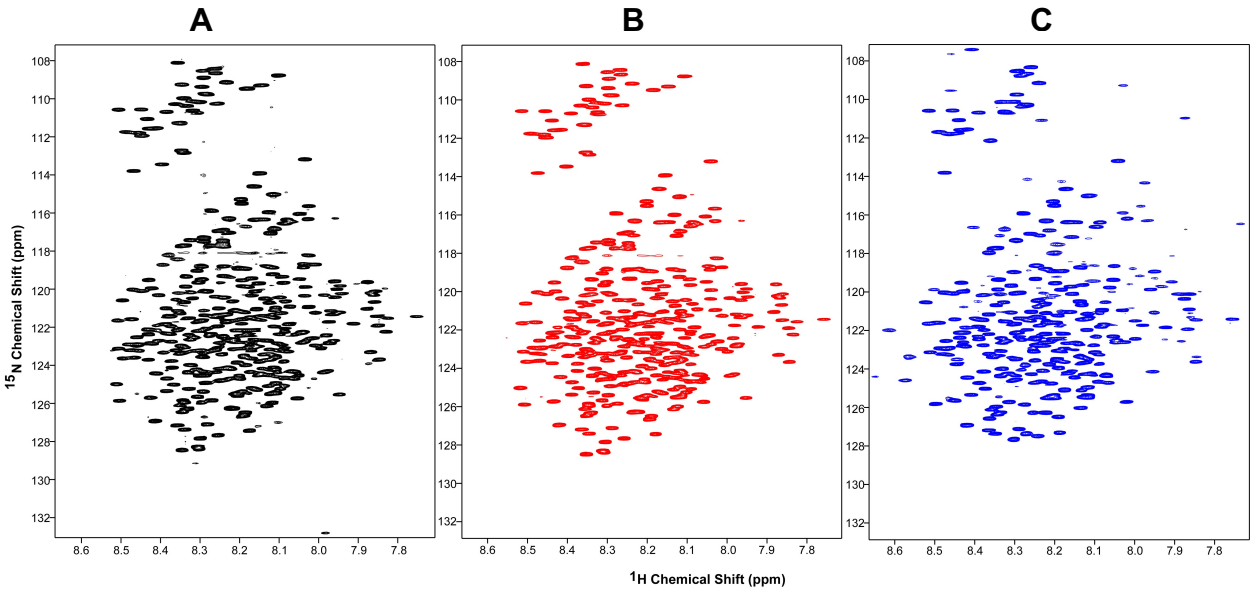

Figure 3-7. Comparison of NMR spectra of ^{15}N-BipC titrated with increasing concentrations of DPC. **(A)** NMR spectrum of 0.2mM BipC in the absence of DPC. **(B)** NMR spectrum of 0.2mM BipC in the presence of 0.5mM DPC. **(C)** NMR spectrum of 0.2mM BipC in the presence of 25mM DPC.

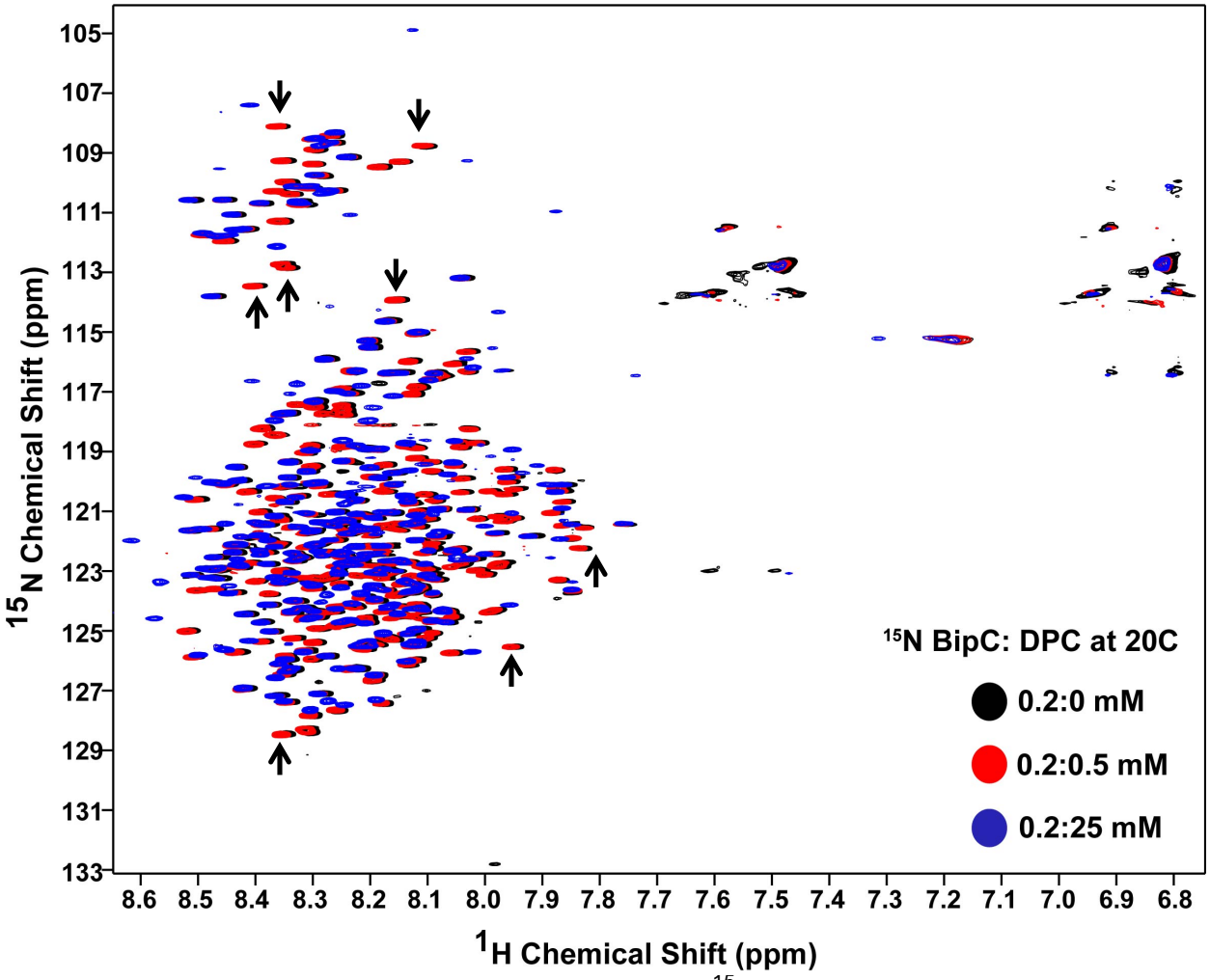

Figure 3-8. Overlay of NMR titrations of ^{15}N-BipC titrated with increasing concentrations of DPC. ^{15}N-BipC titration with 25 mM DPC (above its CMC of 1.1 mM) causes significant conformational change evident from observed shift in peak position and or reduced peak intensity (shown with arrows).

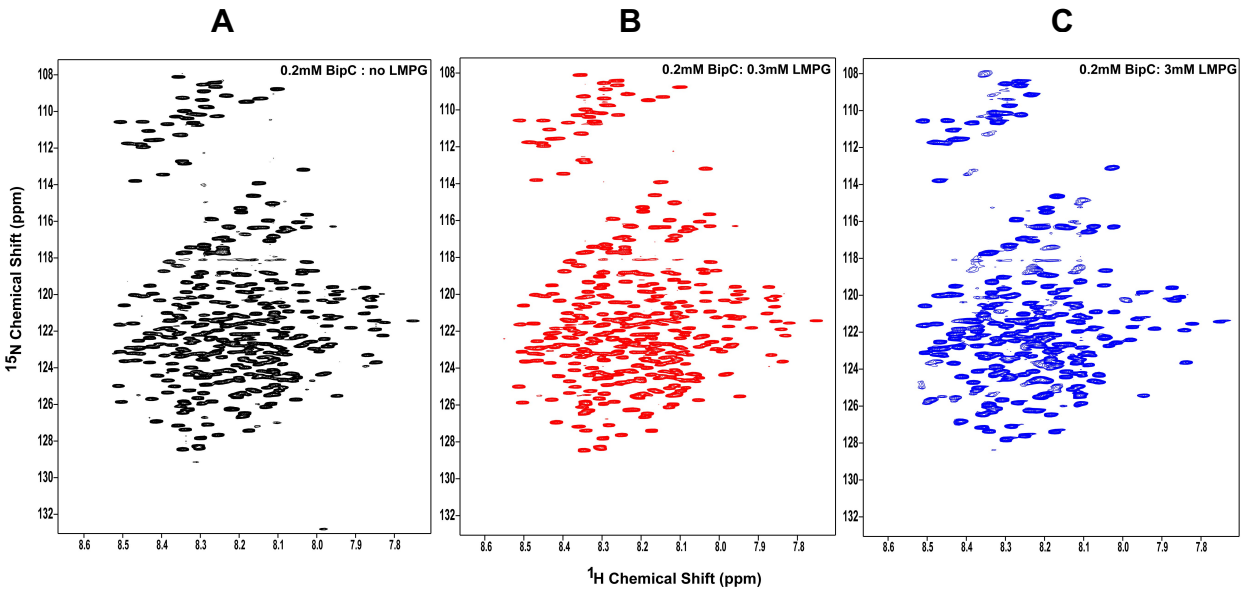

Figure 3-9. Comparison of NMR spectra of ^{15}N-BipC titrated with increasing concentrations of LMPG. **(A)** NMR spectrum of 0.2mM BipC in the absence of LMPG. **(B)** NMR spectrum of 0.2mM BipC in the presence of 0.3mM LMPG. **(C)** NMR spectrum of 0.2mM BipC in the presence of 3mM LMPG.

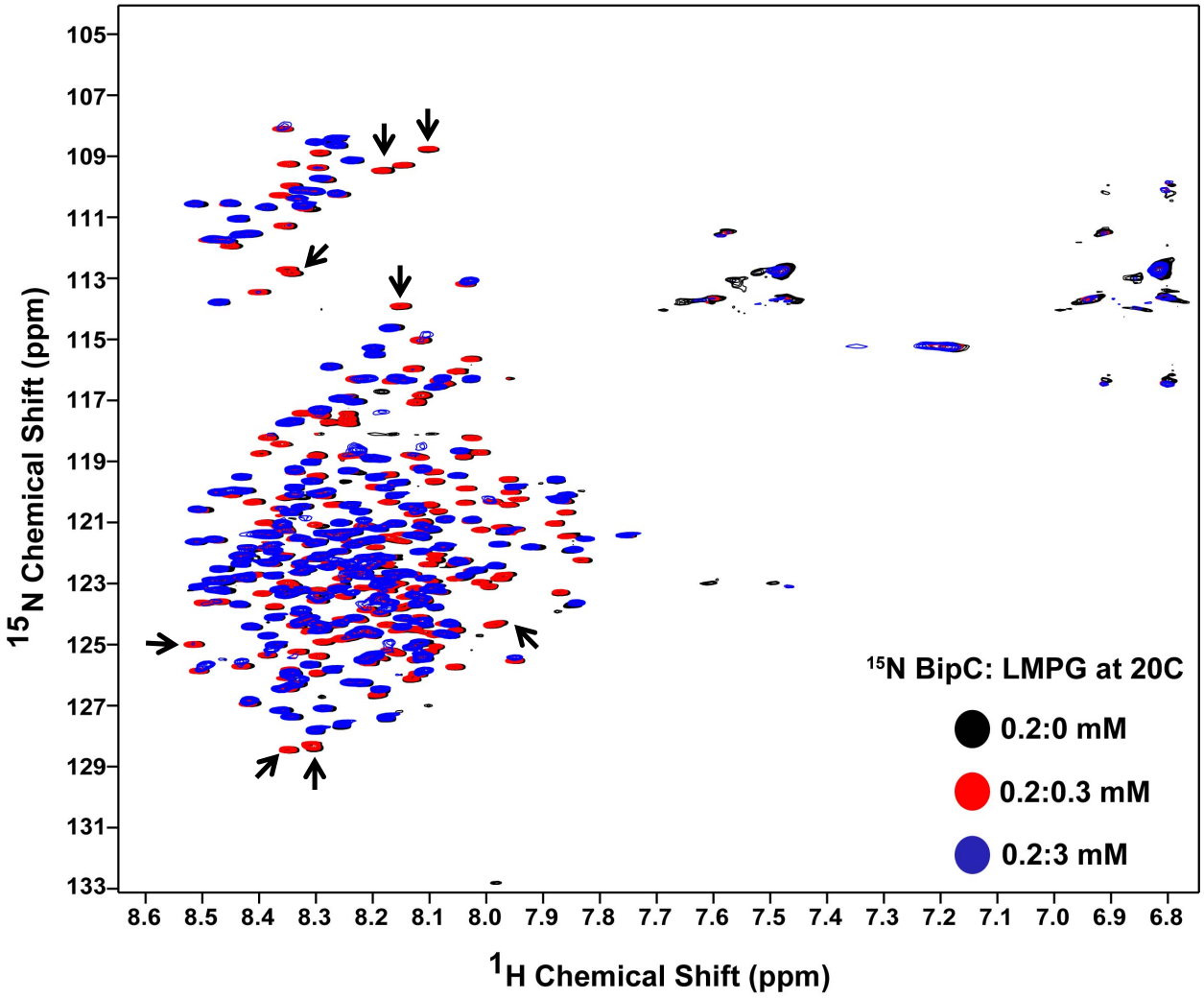

Figure 3-10. Overlay of NMR titrations of ^{15}N-BipC titrated with increasing concentrations of LMPG. ^{15}N-BipC titration with 3 mM DPC (above its CMC of 0.3 mM) causes significant conformational change evident from observed shift in peak position and or reduced peak intensity (shown with arrows).

Table 3-2. Estimation of the secondary structures of BipC by the Dichroweb using the CDSSTR algorithm [17, 18]. **(A)** Secondary structure of BipC in the absence and presence of increasing concentration of DPC. **(B)** Secondary structure of BipC in the absence and presence of increasing concentration of LMPG.

A

DPC conc.	Helix	Strand	Turns	Unordered	Total
0mM DPC	0.10	0.29	0.25	0.34	0.98
0.2mM DPC	0.11	0.30	0.25	0.34	1
1.1mM DPC	0.13	0.28	0.26	0.33	1
5mM DPC	0.37	0.14	0.22	0.27	1
10mM DPC	0.24	0.23	0.23	0.29	0.99
15mM DPC	0.24	0.20	0.26	0.30	1

B

LMPG conc.	Helix	Strand	Turns	Unordered	Total
0mM LMPG	0.09	0.30	0.25	0.35	0.99
0.1mM LMPG	0.13	0.31	0.24	0.32	1
0.3mM LMPG	0.21	0.23	0.27	0.29	1
1mM LMPG	0.38	0.14	0.22	0.27	1.01
3mM LMPG	0.38	0.15	0.21	0.26	1

3.5. References

[1] Attree, O., and Attree, I. (2001) A second type III secretion system in Burkholderia pseudomallei: who is the real culprit?, *Microbiology (Society for General Microbiology) 147*, 3197-3199.

[2] Chatterjee, S., Chaudhury, S., McShan, A. C., Kaur, K., and De Guzman, R. N. (2013) Structure and biophysics of type III secretion in bacteria.(Report), *Biochemistry 52*, 2508-2517.

[3] McShan, A. C. (2015) The Bacterial Type III Secretion System as a Target for Developing New Antibiotics, *Chemical biology & drug design 85*, 30-42.

[4] Myeni, S. K., Wang, L., and Zhou, D. (2013) SipB-SipC complex is essential for translocon formation, *PLoS One 8*, e60499.

[5] Scherer, C. A., Cooper, E., and Miller, S. I. (2000) The Salmonella type III secretion translocon protein SspC is inserted into the epithelial cell plasma membrane upon infection, *Mol Microbiol 37*, 1133-1145.

[6] Kueltzo, L. A., Osiecki, J., Barker, J., Picking, W. L., Ersoy, B., Picking, W. D., and Middaugh, C. R. (2003) Structure- function analysis of invasion plasmid antigen C (IpaC) from Shigella flexneri, *The Journal of biological chemistry 278*, 2792.

[7] Osiecki, J. C., Barker, J., Picking, W. L., Serfis, A. B., Berring, E., Shah, S., Harrington, A., and Picking, W. D. (2001) IpaC from Shigella and SipC from Salmonella possess similar biochemical properties but are functionally distinct, *Molecular Microbiology 42*, 469-481.

[8] Kang, W.-T., Vellasamy, K. M., Chua, E.-G., and Vadivelu, J. (2015) Functional characterizations of effector protein bipc, a type III secretion system protein, in burkholderia pseudomallei pathogenesis.(Report), *211*, 827.

[9] Combet, C., Blanchet, C., Geourjon, C., and Deleage, G. (2000) NPS@: network protein sequence analysis, *Trends Biochem Sci 25*, 147-150.

[10] Kang, C., and Li, Q. (2011) Solution NMR study of integral membrane proteins, *Curr Opin Chem Biol 15*, 560-569.

[11] Kang, C., Tian, C., Sonnichsen, F. D., Smith, J. A., Meiler, J., George, A. L., Jr., Vanoye, C. G., Kim, H. J., and Sanders, C. R. (2008) Structure of KCNE1 and

implications for how it modulates the KCNQ1 potassium channel, *Biochemistry 47*, 7999-8006.

[12] Page, R. C., Moore, J. D., Nguyen, H. B., Sharma, M., Chase, R., Gao, F. P., Mobley, C. K., Sanders, C. R., Ma, L., Sonnichsen, F. D., Lee, S., Howell, S. C., Opella, S. J., and Cross, T. A. (2006) Comprehensive evaluation of solution nuclear magnetic resonance spectroscopy sample preparation for helical integral membrane proteins, *J Struct Funct Genomics 7*, 51-64.

[13] Sanders, C. R., and Sonnichsen, F. (2006) Solution NMR of membrane proteins: practice and challenges, *Magn Reson Chem 44 Spec No*, S24-40.

[14] Cserzö, M., Wallin, E., Simon, I., Von Heijne, G., and Elofsson, A. (1997) Prediction of transmembrane alpha- helices in prokaryotic membrane proteins: the dense alignment surface method, *Protein engineering 10*, 673.

[15] Sievers, F., Wilm, A., Dineen, D., Gibson, T. J., Karplus, K., Li, W., Lopez, R., McWilliam, H., Remmert, M., Söding, J., Thompson, J. D., and Higgins, D. G. (2011) Fast, scalable generation of high- quality protein multiple sequence alignments using Clustal Omega, *Molecular Systems Biology 7*, n/a-n/a.

[16] Robert, X., and Gouet, P. (2014) Deciphering key features in protein structures with the new ENDscript server, *Nucleic Acids Research 42*, W320-W324.

[17] Whitmore, L., and Wallace, B. A. (2004) DICHROWEB, an online server for protein secondary structure analyses from circular dichroism spectroscopic data, *Nucleic Acids Res 32*, W668-673.

[18] Whitmore, L., and Wallace, B. A. (2008) Protein secondary structure analyses from circular dichroism spectroscopy: methods and reference databases, *Biopolymers 89*, 392-400.

[19] Fuguet, E., Ràfols, C., Rosés, M., and Bosch, E. (2005) Critical micelle concentration of surfactants in aqueous buffered and unbuffered systems, *Analytica Chimica Acta 548*, 95-100.

[20] Delaglio, F., Grzesiek, S., Vuister, G. W., Zhu, G., Pfeifer, J., and Bax, A. (1995) NMRPipe: a multidimensional spectral processing system based on UNIX pipes, *J Biomol NMR 6*, 277-293.

[21] Johnson, B. A. (2004) Using NMRView to visualize and analyze the NMR spectra of macromolecules, *Methods Mol Biol 278*, 313-352.

[22] Lau, S. Y., Taneja, A. K., and Hodges, R. S. (1984) Synthesis of a model protein of defined secondary and quaternary structure. Effect of chain length on the stabilization and formation of two- stranded alpha- helical coiled- coils, *The Journal of biological chemistry 259*, 13253.

[23] Mason, J. M., Schmitz, M. A., Muller, K. M., and Arndt, K. M. (2006) Semirational design of Jun-Fos coiled coils with increased affinity: Universal implications for leucine zipper prediction and design, *Proc Natl Acad Sci U S A 103*, 8989-8994.

Chapter 4: Conclusion and Future Directions

The T3SS is a common mechanism utilized by many Gram-negative pathogens to initiate, maintain and spread infection in the host. Some clinically important pathogens that require the assembly of T3SS for infection and the disease associated with them include *Burkholderia pseudomallei* (melioidosis), *Salmonella typhimurium* (gastroenteritis), *Shigella flexneri* (shigellosis), *Pseudomonas aeruginosa* (nosocomial pneumonia), *Yersinia pestis* (plague), *Chlamydia trachomatis* (sexually transmitted disease), and pathogenic strains of *Escherichia coli* called enterohemorrahagic *E. coli* (bloody diarrhea/urinary tract infection) [1]. The emergence of anti-bacterial resistant strains of these pathogens has added another dimension to their versatility of causing infection and threatens the public health immensely around the world [2, 3, 4, 5]. In the current scenario, the exposure of the T3SS on bacterial surface makes it a potential target for developing vaccines and anti-infectives that would disrupt the assembly of the T3SS [6].

In this thesis, I used NMR to investigate the interaction between the *Burkholderia* tip protein BipD and its homologs *Salmonella* SipD and *Shigella* IpaD with the *Burkholderia* minor translocon protein BipC. The outcome of this study suggests that BipC might be binding to the distal region of the tip proteins at the α-β mixed region and perhaps the top part of the coiled-coil domain. This study provides insight about the possible binding site of the minor translocon protein BipC on the tip protein BipD. The result of this study is significant as the binding site of the major translocon in *Salmonella* has been shown to be located on this mixed α-β region [7] and the finding from the

experiments described in this thesis suggests that BipC might also bind near the same interface. This would bring the two translocon proteins spatially in close proximity for interaction with one another essential for the formation of a translocon and T3SS function.

More information is needed to corroborate and validate this finding, and elucidate the tip-translocon interaction and the interaction between the major and the minor translocon proteins. Future experiments may include introducing site-specific point mutations in the mixed α-β region of BipD and studying the interaction with BipC by NMR. Another route would be to assign the NMR spectrum of BipD and BipC that will allow the direct identification of the interacting surface. Cell invasion assays for the wild type and the mutant tip proteins (mutations in the mixed α-β region) will also help establish any disruption in the T3SS assembly and function due to the introduced mutations in that region.

The interaction study of BipC with detergent micelles using NMR suggests that BipC perhaps goes in to the micelle using its single transmembrane domain. This conclusion is based on the observation that as the concentration of the detergents reached above their respective CMC values, there was significant peak broadening and peak loss as seen in the ^{15}N-BipC spectrum (Figure 3-7 and 3-8).

Also, the CD experiments showed significant alterations in the secondary structure of BipC. BipC in the absence of detergents resembles a mostly random coil with partial helical structure whereas in the presence of the detergents it acquired a vastly helical structure apparent from the changes in the BipC CD spectra minima at increasing concentrations of the detergents (Figure 3-5 and 3-6). The initial random coil

structure may indicate the native unfolded structure of BipC in the absence of its chaperone when it is initially secreted through the type III secretory apparatus (T3SA) for assembly. BipC then perhaps acquires a helical structure upon insertion into a membrane-like environment.

Overall this study provided evidence supporting a major conformational and structural shift in BipC in the presence of membrane mimetic detergents. This calls for a functional assay where the binding activity of BipC can be compared in the presence and absence of a suitable membrane mimic. The binding of BipC to the tip protein BipD or the major translocon BipB can be studied in detergent micelles by electron paramagnetic resonance (EPR) spectroscopy or fluorescence spectroscopy methods, which are more sensitive than NMR. This will require site-directed mutagenesis to introduce cysteine point mutations for label attachment, a fluorophore label for fluorescence or a MTSL spin label for EPR analysis. These interaction studies will shed light on the impact of the structural changes of BipC on its ability to bind to other proteins required for the assembly of a functional T3SS.

References

[1] Coburn, B., Sekirov, I., and Finlay, B. B. (2007) Type III secretion systems and disease, *Clin Microbiol Rev 20*, 535-549.

[2] Kotloff, K. L., Nataro, J. P., Blackwelder, W. C., Nasrin, D., Farag, T. H., Panchalingam, S., Wu, Y., Sow, S. O., Sur, D., Breiman, R. F., Faruque, A. S., Zaidi, A. K., Saha, D., Alonso, P. L., Tamboura, B., Sanogo, D., Onwuchekwa, U., Manna, B., Ramamurthy, T., Kanungo, S., Ochieng, J. B., Omore, R., Oundo, J. O., Hossain, A., Das, S. K., Ahmed, S., Qureshi, S., Quadri, F., Adegbola, R. A., Antonio, M., Hossain, M. J., Akinsola, A., Mandomando, I., Nhampossa, T., Acacio, S., Biswas, K., O'Reilly, C. E., Mintz, E. D., Berkeley, L. Y., Muhsen, K., Sommerfelt, H., Robins-Browne, R. M., and Levine, M. M. (2013) Burden and aetiology of diarrhoeal disease in infants and young children in developing countries (the Global Enteric Multicenter Study, GEMS): a prospective, case-control study, *Lancet 382*, 209-222.

[3] Allen, H. K., Donato, J., Wang, H. H., Cloud-Hansen, K. A., Davies, J., and Handelsman, J. (2010) Call of the wild: antibiotic resistance genes in natural environments, *Nat Rev Microbiol 8*, 251-259.

[4] Wellington, E. M., Boxall, A. B., Cross, P., Feil, E. J., Gaze, W. H., Hawkey, P. M., Johnson-Rollings, A. S., Jones, D. L., Lee, N. M., Otten, W., Thomas, C. M., and Williams, A. P. (2013) The role of the natural environment in the emergence of antibiotic resistance in gram-negative bacteria, *Lancet Infect Dis 13*, 155-165.

[5] Davies, J., and Davies, D. (2010) Origins and evolution of antibiotic resistance, *Microbiol Mol Biol Rev 74*, 417-433.

[6] Jneid, B., Moreau, K., Plaisance, M., Rouaix, A., Dano, J., and Simon, S. (2016) Role of T3SS-1 SipD Protein in Protecting Mice against Non-typhoidal Salmonella Typhimurium, *PLoS Negl Trop Dis 10*, e0005207.

[7] McShan, A. C., Kaur, K., Chatterjee, S., Knight, K. M., and De Guzman, R. N. (2016) NMR identification of the binding surfaces involved in the Salmonella and Shigella Type III secretion tip-translocon protein-protein interactions, *Proteins 84*, 1097-1107.

Addendum: Interaction of *Pseudomonas aeruginosa* minor translocon protein PopD with detergents

A.1. Introduction

Pseudomonas aeruginosa is an opportunistic Gram-negative pathogen and a causative agent of nosocomial infections in immunocompromised patients [1]. *Pseudomonas aeruginosa* employs the T3SS to cause acute or chronic infection in the host and multidrug resistance in *Pseudomonas* has become a major impediment in the treatment of infected patients [1] . Due to the critical role of T3SS in virulence and its exposure on the bacterial surface, it is an appealing target for novel therapeutics development [2]. Targeting T3SS would also lessen the selection pressure on the bacteria for drug resistance as it would render the bacteria avirulent rather than having a bactericidal effect [3]. This strategy would also be beneficial to the preservation of normal flora that are essential in keeping the pathogens in check [3].

Structural and interaction studies in *Shigella*, *Pseudomonas*, and *Yersinia* have revealed that the major and minor translocon proteins of the T3SS might bind to the same binding region on their common chaperones [4, 5]. Still, the structure of *Pseudomonas* minor translocon protein PopD and its interaction with membrane is unknown. The NMR study of the translocon proteins is limited because of lack of good NMR data, which could be due to their large size, intrinsically disordered regions, dynamics due to intrinsic flexibility, and the absence of their natural membrane environment [6, 7]. This chapter examines into the interaction of PopD with membrane

mimic detergents by NMR spectroscopy with the future goal of studying protein-protein interaction.

A.2. Experimental Section

A.2.1. Expression and purification of ^{15}N-PopD

PopD and its chaperone PcrH were previously sub-cloned into pET-DUET1 [8] by a graduate student in the lab (Dr. Andrew McShan) based on a previously reported protocol [8]. The plasmid construct had an N-terminal His_6 fused to PcrH subcloned in multiple cloning site 1 (MCS1) and PopD in MCS2. PcrH-PopD complex was expressed in *E. coli* BL21 (DE3) DNAY cells in 1 L of 1X M9 minimal media with 100 ug/mL carbenicillin and 30 ug/mL kanamycin for antibiotic selection supplemented with 1 g/L ^{15}NH4Cl for uniform amide backbone labeling. The cells were grown at 37 °C until an OD_{600}~0.8 after which the protein expression was induced with 0.5 mM IPTG overnight at 15 °C. Bacterial cells were harvested by centrifugation at ~4000 rpm for 10 min, re-suspended in binding buffer (20 mM Tris-HCl, 5 mM imidazole, 500 mM NaCl, pH 8.0, and 0.2mM phenylmethanesulfonyl fluoride), and lysed by sonication on ice. Cell debris were removed by centrifugation at 13000 rpm for ~10 min with 0.1 mM PEI solution. The soluble PopD-PcrH complex was purified by gravity flow using Ni^{2+}-affinity chromatography on Ni-NTA (nickel-nitrilotriacetic acid) resin packed column. The complex was separated by incubation in binding buffer containing 6 M urea overnight followed by stepwise complete removal of urea using binding buffer containing decreasing concentration of urea. The separated proteins were purified again by Ni^{2+}-

affinity chromatography. The purified PopD was pooled, dialyzed into NMR buffer and concentrated using Amicon Ultra 3K filtration units. The protein concentration was determined by reading the absorbance at 280 nm.

A.2.2. Secondary structure prediction

The secondary structure of PopD was predicted using the NPS@ web server. The consensus secondary structure prediction was based on the results of four algorithms DSC, MLRC, PHD, and Predator.

A.2.3. NMR experiments

NMR data were acquired on a Bruker Advance 800 MHz spectrometer with a cryogenic triple resonance probe. The protein concentration used for all experiments was 0.4 mM. The typical acquisition parameters were 2048 ^{15}N complex points, 128 ^{1}H complex points, 48 scans at 30 °C. The sweep width for ^{15}N was 30 ppm centered at 118 ppm and for ^{1}H it was 18 ppm centered at 4.7 ppm. NMR data were processed using NMRPipe [9] and analyzed using NMRView [10].

A.3. Results

A.3.1. Expression and purification of ^{15}N-PopD

PopD and PcrH were co-expressed from a pET-DUET expression system that yielded good expression of the proteins. After first Ni^{2+}-affinity purification, the complex was subjected to separation in the presence of 6 M urea. After the separation, the

protein solution was purified again and the minor translcon protein PopD was collected in Wash fraction with 5 mM imidazole while His_6-PcrH was collected in the Elution fraction with 250 mM imidazole. The purified protein was verified by SDS PAGE and coomassie blue staining methods as well as by mass spectrometry (Figure A1 and A2).

A.3.2. Secondary structure prediction

The online web server NPS@ was employed to predicted a consensus secondary structure using four different algorithms [11]. PopD is predicted to be predominantly α-helical. The N-terminal PopD is predicted to contain higher percentage of random coil suggesting disordered region while the C-terminal region is more structured and helical (Figure A3).

A.3.3. NMR study of PopD interaction with detergents

PopD yielded a collapsed NMR spectrum with chemical shift dispersion > 1 ppm in the absence of detergents (Figure A4). The NMR also didn't produce peaks for all the amino acids of PopD. NMR titration of PopD with 25 mM DPC (above CMC of 1.1 mM) slightly improved the peak resolution and increased the number of peaks observed. As PopD was titrated with even higher concentration of DPC (~200 mM), the NMR spectrum showed further improvement in peak resolution and increased number of observed peaks. Two trp residues were also observed in the presence of DPC detergent above its CMC concentration (Figure A5).

A.4. Discussion

Minor translocon proteins are membrane associated proteins and are difficult to express in soluble form. Others have shown that minor translocon proteins express in the soluble fraction as a complex with native chaperone proteins [8]. Therefore, PopD was expressed from a bicistronic construct in pET-DUET1 vector [8, 12, 13]. The co-expression of PopD and PcrH allowed good expression of PopD. The complex was separated using 6M urea [8] that was verified by SDS-PAGE (Figure A1) and mass spectrometry analysis (Figure A2).

The NMR experiment of PopD in the absence and presence of the detergent, DPC were acquired and compared. PopD in the absence of DPC shows narrow chemical shift dispersion (Figure A4) and significant numbers of amide peaks were missing from the spectrum characteristic of partially folded or helical proteins lacking significant tertiary fold [14]. The absence of majority of the amide peaks and poor resolution could be due to the presence of significant disordered regions in PopD, intrinsic dynamics due to flexibility, and the absence of chaperones or membrane environment to stabilize the structure. This is supported by the secondary structure prediction result, which shows PopD to vastly consist of random coil at the extreme N-terminal region (Figure A3). One possible solution could be to truncate the protein at the terminal ends to observe any improvement in its NMR spectrum. Reconstitution of PopD into DPC micelles improved the peak resolution and yielded a greater number of observed peaks but still more than half of PopD peaks were not observed. The visualization of the two tryptophan residues suggests a conformational change and a probable gain of some structure in the detergent micelles (Figure A5).

Future experiments to address the difficulties in the above experiments would be to screen a number of detergents or detergent-lipid mixtures to get a good quality NMR data. Also, other labeling strategies such as ILV-labeling or specific amino acid amide or side chain labeling could aid in the identification of the NMR peaks. Determination of a suitable membrane mimic would be a critical step for structural and interaction studies of PopD with the other components of *Pseudomonas* T3SS.

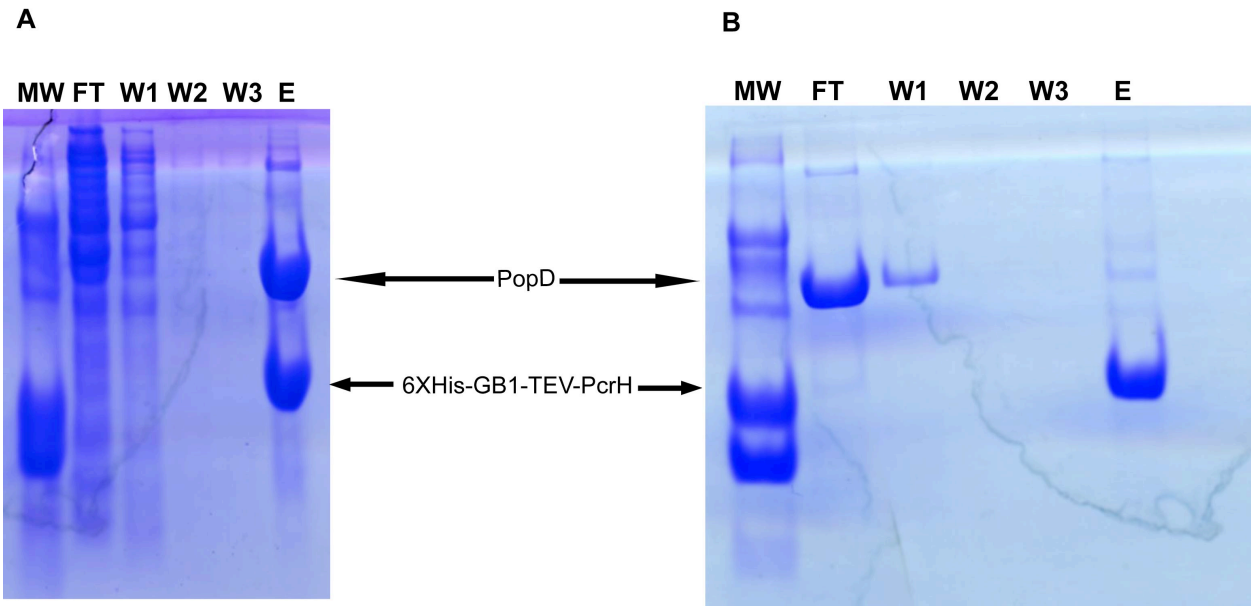

Figure A1. Purification Gel of PopD. **(A)** First Ni^{2+}- affinity purification of PopD-PcrH complex. **(B)** Second Ni^{2+}- affinity purification of PopD after denaturation step to separate the PopD-PcrH complex. (MW= ladder, FT= flow through, W1= wash1, W2= wash2, W3= wash3, E= elution. Molecular weight of PopD= 31.3kDa and PcrH= 19.5kDa).

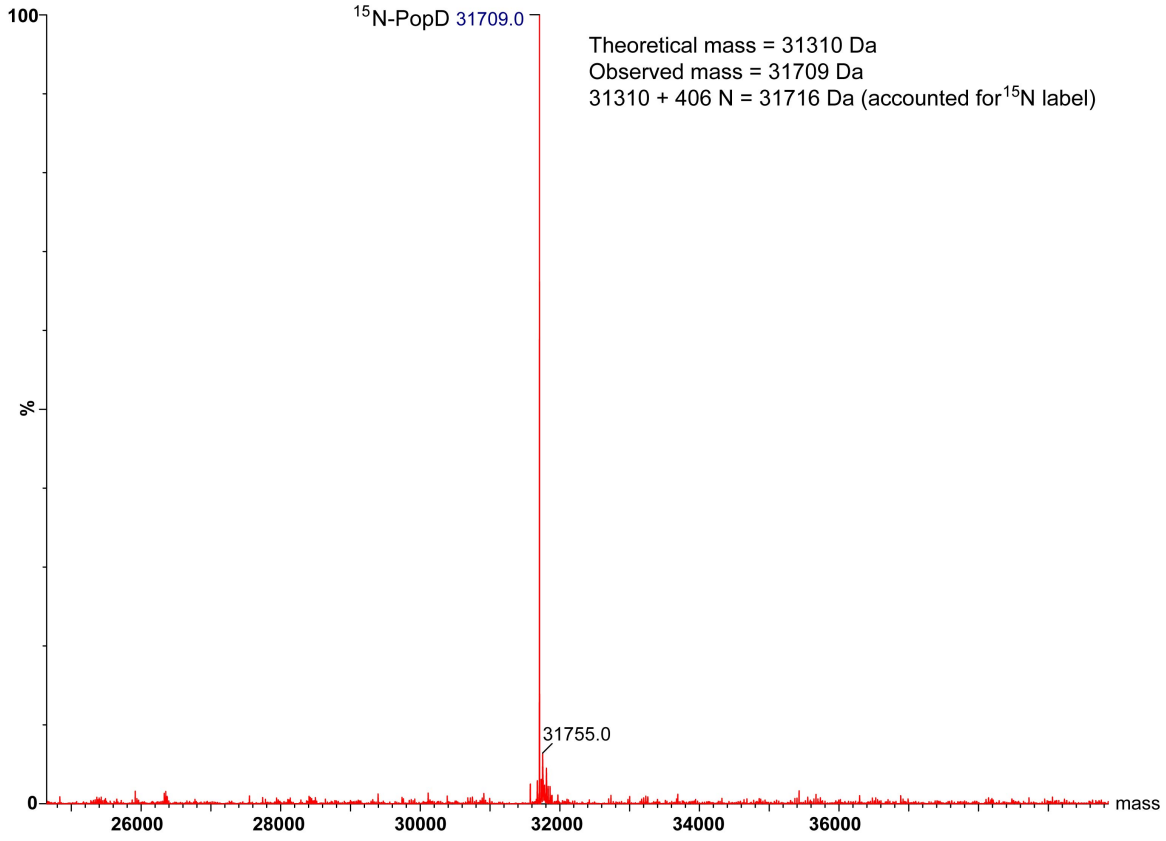

Figure A2. Electrospray ionization mass spectrometry to verify PopD purification. The theoretical and observed mass of PopD is shown in the figure to account for the difference in the mass due to ^{15}N labeling of PopD.

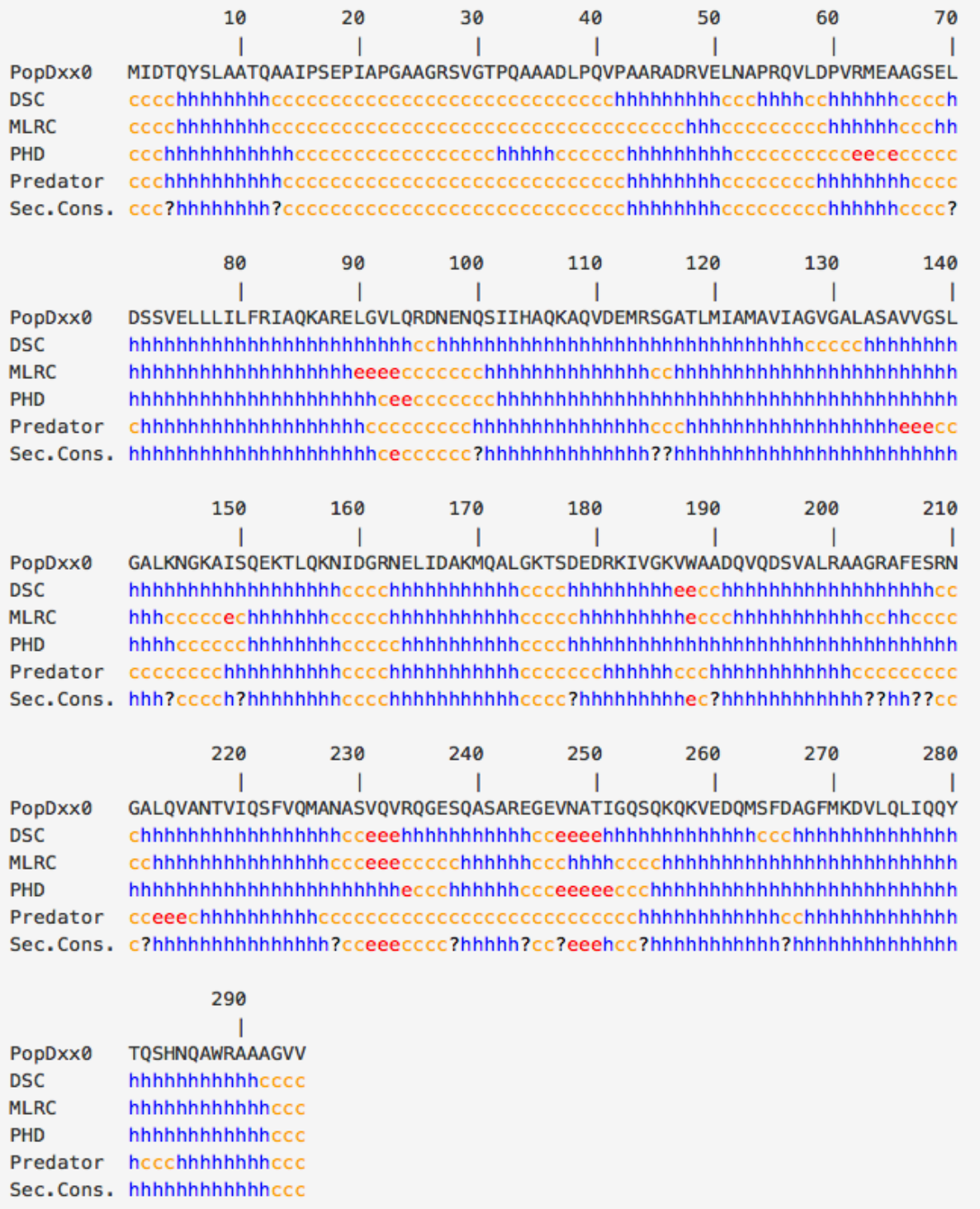

Figure A3. Secondary structure prediction of PopD from *Pseudomonas aeruginosa*. Secondary structure of PopD is predicted using NPS@ Web server employing four algorithms DSC, MLRC, PHD, Predator, and a consensus structure from all four algorithms is shown [11].

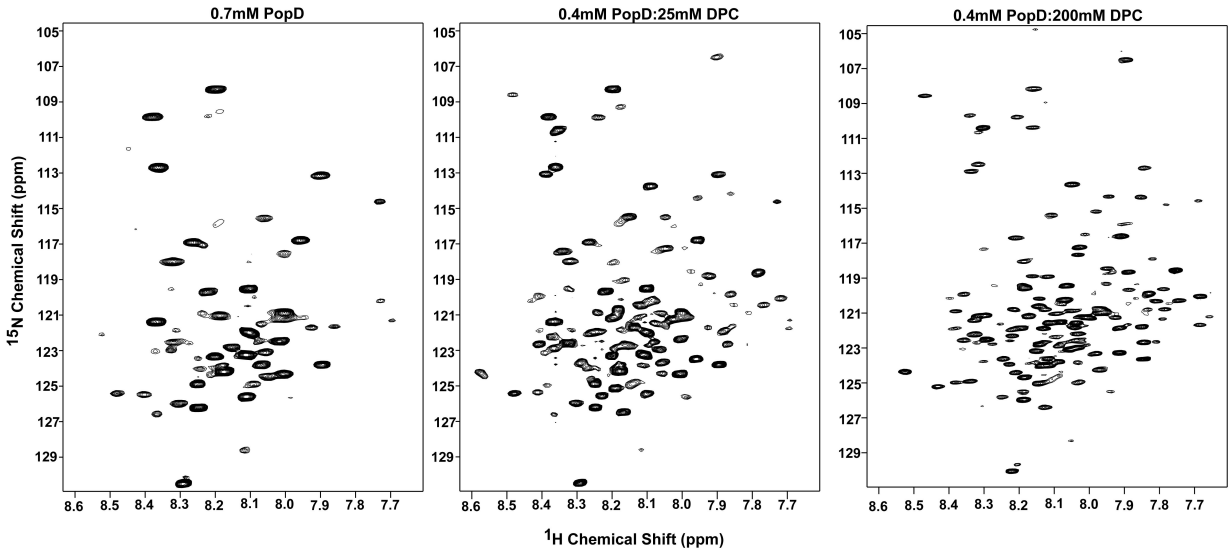

Figure A4. Comparison of NMR spectra of ^{15}N-PopD titrated with DPC at 30 °C. ^{15}N-PopD in the absence of DPC (left panel), ^{15}N-PopD titrated with 25mM of DPC (middle panel), and ^{15}N-PopD titrated with 200mM DPC (right panel).

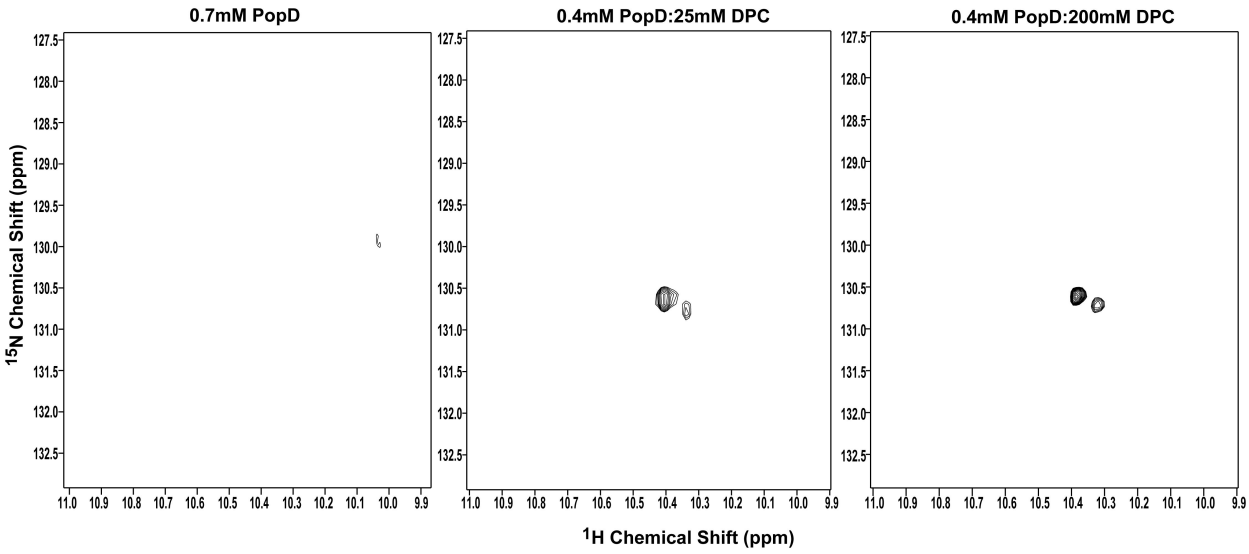

Figure A5. Comparison of NMR spectra of ^{15}N-PopD titrated with DPC at 30 °C showing the tryptophan residues. ^{15}N-PopD in the absence of DPC (left panel), ^{15}N-PopD titrated with 25mM of DPC (middle panel), and ^{15}N-PopD titrated with 200mM DPC (right panel).

A.5. References

[1] Anantharajah, A., Mingeot-Leclercq, M. P., and Van Bambeke, F. (2016) Targeting the Type Three Secretion System in Pseudomonas aeruginosa, *Trends Pharmacol Sci 37*, 734-749.

[2] Ramirez-Estrada, S., Borgatta, B., and Rello, J. (2016) Pseudomonas aeruginosa ventilator-associated pneumonia management, *Infect Drug Resist 9*, 7-18.

[3] Rasko, D. A., and Sperandio, V. (2010) Anti-virulence strategies to combat bacteria-mediated disease, *Nat Rev Drug Discov 9*, 117-128.

[4] Lunelli, M., Lokareddy, R. K., Zychlinsky, A., and Kolbe, M. (2009) IpaB-IpgC interaction defines binding motif for type III secretion translocator, *Proc Natl Acad Sci U S A 106*, 9661-9666.

[5] Schreiner, M., and Niemann, H. H. (2012) Crystal structure of the Yersinia enterocolitica type III secretion chaperone SycD in complex with a peptide of the minor translocator YopD, *BMC Struct Biol 12*, 13.

[6] Fernandez, C., and Wider, G. (2003) TROSY in NMR studies of the structure and function of large biological macromolecules, *Curr Opin Struct Biol 13*, 570-580.

[7] Sanders, C. R., and Sonnichsen, F. (2006) Solution NMR of membrane proteins: practice and challenges, *Magn Reson Chem 44 Spec No*, S24-40.

[8] Romano, F. B., Rossi, K. C., Savva, C. G., Holzenburg, A., Clerico, E. M., and Heuck, A. P. (2011) Efficient isolation of Pseudomonas aeruginosa type III secretion translocators and assembly of heteromeric transmembrane pores in model membranes, *Biochemistry 50*, 7117-7131.

[9] Delaglio, F., Grzesiek, S., Vuister, G. W., Zhu, G., Pfeifer, J., and Bax, A. (1995) NMRPipe: a multidimensional spectral processing system based on UNIX pipes, *J Biomol NMR 6*, 277-293.

[10] Johnson, B. A. (2004) Using NMRView to visualize and analyze the NMR spectra of macromolecules, *Methods Mol Biol 278*, 313-352.

[11] Combet, C., Blanchet, C., Geourjon, C., and Deleage, G. (2000) NPS@: network protein sequence analysis, *Trends Biochem Sci 25*, 147-150.

[12] Faudry, E., Job, V., Dessen, A., Attree, I., and Forge, V. (2007) Type III secretion system translocator has a molten globule conformation both in its free and chaperone-bound forms, *FEBS J 274*, 3601-3610.

[13] Schoehn, G., Di Guilmi, A. M., Lemaire, D., Attree, I., Weissenhorn, W., and Dessen, A. (2003) Oligomerization of type III secretion proteins PopB and PopD precedes pore formation in Pseudomonas, *EMBO J 22*, 4957-4967.

[14] Kang, C., and Li, Q. (2011) Solution NMR study of integral membrane proteins, *Curr Opin Chem Biol 15*, 560-569.